

Large-Scale Dynamos and Magnetic Helicity: Principles and Relevance to Coronae, Outflows, and Laboratory Plasmas

Eric G. Blackman¹

¹*Department of Physics and Astronomy, University of Rochester, Rochester NY, 14627, USA*

Dynamos are studied by astrophysical, planetary, and fusion communities but the differences between dynamo types can be a source of confusion. To elucidate the relationship between the different dynamos, I divide dynamos into three categories e.g. [1]: 1. Nonhelical flow-driven dynamos which amplify fields on scales at or below the driving turbulence; 2. Helical flow-driven dynamos which amplify or sustain large scale magnetic fields in an otherwise turbulent flow. Traditional stellar, planetary, and Galactic dynamos aimed at explaining cycle periods and large-scale fields fit into this category; 3. Magnetically dominated helical dynamos, which sustain the large-scale magnetic field against resistive decay and evolve the magnetic geometry toward the lowest energy state. All three types occur in astrophysics whereas laboratory plasma dynamos in fusion devices are of type 3. Type 1 dynamos requires no helicity of any kind.

Focusing on type 2 and 3 dynamos, which both require a mean magnetic field aligned electromotive force, I will then discuss how different limits of a unified set of equations for magnetic helicity evolution reveal simple dynamos of both types. Dynamos that systematically amplify or sustain fields on spatial or temporal scales larger than those of the fluctuations involve a spatial or spectral transfer of magnetic helicity. (first apparent in Ref. [2] for type 2 dynamos.) Examples of steady-state vs. time dependent dynamos in the presence and absence of boundary terms and the influence on dynamo saturation will be discussed. For the simplest closed volume cases, type 2 dynamos involve the spectral segregation of opposite signs of magnetic helicity, while type 3 dynamos involve transport of net magnetic helicity from small to large scales.

The magnetic helicity framework and associated results are part of a growing body of work that reflects how magnetic helicity has emerged as a useful tool for understanding the operation and nonlinear evolution of large-scale dynamos (see [3] for a review). It is important to distinguish practical modeling of planetary and stellar dynamos, where the immediate aim is to specifically reproduce observations, from idealized studies of simple dynamos aimed at understanding the theoretical principles of nonlinear saturation. It is hoped that insights gained from the latter can eventually be incorporated into the former.

In this context, idealized type 2 MHD dynamo simulations of α^2 dynamos in periodic boxes by several groups e.g. [4, 5] have shown that when MHD turbulence is forced with sufficient kinetic helicity, the saturated magnetic energy spectrum evolves from having a single peak below the forcing scale to become doubly peaked, with one peak at the system (= largest) scale and one at the forcing scale. If we are eventually to understand the nonlinear saturation in a realistic helical dynamo with a practical theory, we should assess whether such a theoretical framework can first explain the saturation in simple numerical experiments. Toward this end, finite scale approximations to the dynamical evolution of the magnetic spectra have proven to be useful. Simple two scale dynamical models incorporating magnetic helicity evolution capture saturation quite well [6]. However, modeling the relative shift of the small-scale magnetic peak with respect to the small scale velocity peak at early times requires at least a three scale helical dynamo theory [7]. The three scale approach does show that the small-scale helical magnetic energy first saturates at very small scales, but then successively saturates at larger values at larger scales, eventually becoming dominated by the forcing scale. The transfer of the small-scale peak to the forcing scale is completed by the end of the kinematic growth regime of the large-scale field, and does not depend on magnetic Reynolds number R_M for large R_M . The three and two-scale theories evolve almost identically at late times, both consistent with the late time doubly humped “camel” magnetic spectra seen in simulations.

Next I will discuss how type 2 and type 3 dynamos can act together in a two-stage helical dynamo framework for growing the large-scale magnetic fields of coronal cycles, coronal holes, and astrophysical jets [8]. Jet and coronal hole fields are of large scale with respect to that of their anchoring rotators and in both stars and disks, and these fields are unlikely to result from simple flux accretion from the material that formed the rotator: In the sun, the solar cycle reversals prove that the field must be regenerated in situ. In disks, the field can diffuse faster than it is accreted in the absence of in situ generation.

The two stage, large-scale field formation paradigm is this: First, a type 2 velocity driven helical dynamo amplifies fields of large enough scale that they buoyantly rise and supply magnetic helicity to the corona [9, 10] without being shredded by turbulent diffusion. Once in the corona, continued footpoint motions can further twist the field and inject more magnetic helicity. The loops respond by rising or opening to larger scales. Coronal mass ejection (CME) type events can be associated with this evolution if instability occurs. Such field evolution in the corona is in fact a type 3 dynamo. Disks and stars act as helicity injecting boundaries to their magnetically dominated corona, a circumstance directly analogous to Spheromak formation in the laboratory. In short, global fields of stars and disk involve a type 2 dynamo inside the rotator, which injects magnetic helicity into a type 3 dynamo in the corona. Note that we observe the exterior field, not the interior field for all astrophysical rotators except our Galaxy.

Finally, I will briefly mention some work on interface dynamos in supernovae [11]. For protosupernovae unlike the sun, the backreaction on the differential rotation is important in limiting the lifetime of the dynamo. These supernovae interface dynamos are explosive, not steady, and highlight processes that might account for the observed bipolar outflow asymmetry in explosive end states of stars.

References

- [1] E.G. Blackman & H. Ji, 2006, in press MNRAS, astro-ph/0604221 *Laboratory Plasma Dynamos, Astrophysical Dynamos, and Magnetic Helicity Evolution*
- [2] A. Pouquet, U. Frisch, J. Léorat, J. Fluid Mech., **77** 321 (1976) *Strong MHD helical turbulence and the nonlinear dynamo effect*
- [3] A. Brandenburg, & K. Subramanian, K. 2005, Physics Reports, 417, 1, *Astrophysical magnetic fields and nonlinear dynamo theory*
- [4] A. Brandenburg, 2001, ApJ, 550, 824, *The Inverse Cascade and Nonlinear Alpha-Effect in Simulations of Isotropic Helical Hydromagnetic Turbulence*
- [5] J. Maron & E.G. Blackman 2002, ApJL, 566, L41, *Effect of Fractional Kinetic Helicity on Turbulent Magnetic Dynamo Spectra*
- [6] E.G. Blackman & G.B. Field 2002, Physical Review Letters, 89, 265007, *New Dynamical Mean-Field Dynamo Theory and Closure Approach*
- [7] E.G. Blackman, 2003, MNRAS, 344, 707, *Understanding helical magnetic dynamo spectra with a nonlinear four-scale theory*
- [8] E.G. Blackman, 2005, Physics of Plasmas, 12, 2304, *Bihelical Magnetic Relaxation and Large Scale Magnetic Field Growth*
- [9] E.G. Blackman, & G.B. Field, 2000, MNRAS, 318, 724 *Coronal Activity from Dynamos in Astrophysical Rotators*
- [10] E.G. Blackman & A. Brandenburg, 2003, ApJL, 584, L99 *Doubly Helical Coronal Ejections from Dynamos and Their Role in Sustaining the Solar Cycle*
- [11] E.G. Blackman, J.T. Nordhaus, & J.H. Thomas, 2006, New Astronomy, 11, 452, *Extracting rotational energy in supernova progenitors: Transient Poynting flux growth vs. turbulent dissipation*

Critical issues to get right about stellar dynamos

Axel Brandenburg

NORDITA, Blegdamsvej 17, DK-2100 Copenhagen Ø, Denmark

Small scale versus large scale dynamos. A good definition of large scale and small scale dynamos is not available. For now, let us say that small scale dynamos have no mean flow ($\overline{\mathbf{U}} = 0$) and produce no mean field ($\overline{\mathbf{B}} = 0$). Here we reserve ourselves some freedom in the definition of meaningful averages (ensemble, time, or spatial averages over one or two coordinate directions, depending on the nature of the problem). Large scale dynamos produce a mean field ($\overline{\mathbf{B}} \neq 0$), but may or may not have a mean flow ($\alpha\Omega$ and $\overline{\mathbf{W}} \times \overline{\mathbf{J}}$ versus α^2 dynamos, for example). By this definition, dynamos in Taylor-Green flows [1] do have a finite time-averaged flow and would not be small scale dynamos.

Large scale dynamos. All known large scale dynamos ($\alpha\Omega$, $\overline{\mathbf{W}} \times \overline{\mathbf{J}}$, and α^2 dynamos) produce magnetic helicity, which reacts back on the dynamo. As a consequence, the mean field saturates at a low value, $\overline{\mathbf{B}}^2 \ll B_{\text{eq}}^2 \equiv \langle \mu_0 \rho \mathbf{u}^2 \rangle$. It is demonstrated (Fig. 1) that, by allowing for magnetic helicity fluxes out of the domain, the large scale field is able to saturate at equipartition field strength.

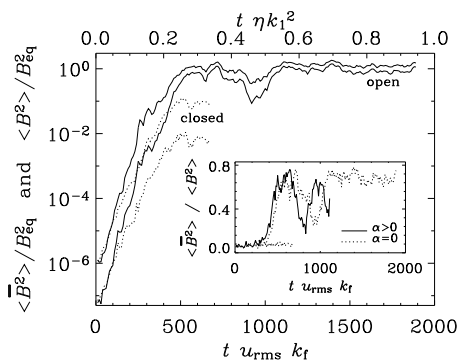


Figure 1: Evolution of the energies of the total field $\langle \mathbf{B}^2 \rangle$ and of the mean field $\langle \overline{\mathbf{B}}^2 \rangle$, in units of B_{eq}^2 , for runs with non-helical forcing and open or closed boundaries; see the solid and dotted lines, respectively. The inset shows a comparison of the ratio $\langle \overline{\mathbf{B}}^2 \rangle / \langle \mathbf{B}^2 \rangle$ for nonhelical ($\alpha = 0$) and helical ($\alpha > 0$) runs. For the nonhelical case the run with closed boundaries is also shown (dotted line near $\langle \overline{\mathbf{B}}^2 \rangle / \langle \mathbf{B}^2 \rangle \approx 0.07$). Adapted from Ref. [2].

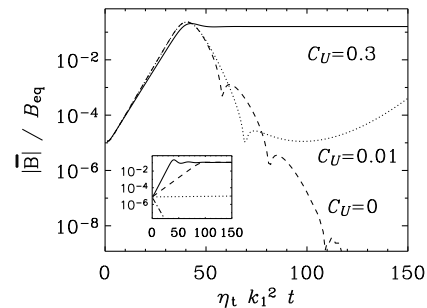


Figure 2: Evolution of the field strength obtained by solving the mean field equations with vertical advection (solid line, $C_U = 0.3$) and without it (dashed line, $C_U = 0$). Here, $C_U = |\overline{\mathbf{U}}|_{\text{max}} / (\eta_t k_1)$ is a nondimensional measure of the strength of advection out of the dynamo domain. The dotted curve, obtained for $C_U \ll 1$, shows that even weak advection can affect the long-term evolution of magnetic field. The inset shows similar results for $C_U = 0.1$ (solid), 1.5 (dashed), 2 (dotted) and 3 (dash-dotted). Adapted from Ref. [3].

The results of simulations are qualitatively, and in some cases also quantitatively, well reproduced by mean field models where the effect of magnetic helicity fluxes enters into the dynamical feedback formula for the magnetic alpha effect (even when there is no kinetic alpha effect!).

Magnetic helicity fluxes that are known to work include the shear-driven Vishniac-Cho flux [4, 5, 6], which can be written in the form $\overline{\mathbf{F}} \propto (\overline{\mathbf{S}} \overline{\mathbf{B}}) \times \overline{\mathbf{B}}$ and an advectively driven flux [3] of the form $\overline{\mathbf{F}} \propto \alpha_M \overline{\mathbf{U}}$,

where α_M is the magnetic α effect. The former is the one operating predominantly in the simulations in Fig. 1, while the latter one operates in the mean field model shown in Fig. 2.

Small scale dynamos. An explanation is in order as to why simulations of dynamo action in spherical shells may not yet have shown strong large scale dynamos. The simulations of Brun et al. [7] show dynamo action at unit magnetic Prandtl number ($\text{Pr}_M = 1$). As the value of Pr_M is decreased, one must increase the fluid Reynolds number Re at least by the same amount to maintain the same magnetic Reynolds number R_m , but this is already prohibitively expensive. Solar-like simulations at $\text{Pr}_M < 1$ have not yet been considered, but it is conceivable that the critical magnetic Reynolds number, $R_{m,\text{crit}}$, increases with decreasing Pr_M , as is found for typical small scale dynamos with zero mean flow [8]. Thus, the tentative suggestion is that the simulations of Brun et al. show dynamo action that belongs to the class of small scale dynamos (even though they do have a mean flow). This type of dynamo action would go away for smaller value of Pr_M , provided they value of R_m is still not very large. At the same time, the large scale dynamo effect may still be sub-critical, i.e. shear and the effective α , or some other large scale effect, are still too weak, and the effective turbulent diffusivity is still too large.

Implications for LES. The indications are that, at low values of Pr_M , when the values of Rm are still small enough to allow a direct simulation of the induction equation, LES (including less advanced “tricks” such as Smagorinsky and hyper viscosity) for the momentum equation, produce accurate results [8] for the onset of dynamo action. However, similar approaches for the magnetic field are difficult and often not successful [9, 10]. Successful LESs for MHD would need to incorporate magnetic helicity fluxes (for large scale dynamos) and must somehow incorporate the fast growth at the Kazantsev (resistive) scale (for small scale dynamos).

References

- [1] Y. Ponty, P. D. Mininni, D. C. Montgomery, J.-F. Pinton, H. Politano, A. Pouquet 2005. *Numerical Study of Dynamo Action at Low Magnetic Prandtl Numbers*, Phys. Rev. Lett. **94**, 164502.
- [2] A. Brandenburg 2005. *The case for a distributed solar dynamo shaped by near-surface shear*, Astrophys. J. **625**, 539 – 547.
- [3] A. Shukurov, D. Sokoloff, K. Subramanian and A. Brandenburg 2006. *Galactic dynamo and helicity losses through fountain flow*, Astron. Astrophys. **448**, L33 – L36.
- [4] E. T. Vishniac and J. Cho 2001. *Magnetic helicity conservation and astrophysical dynamos*, Astrophys. J. **550**, 752 – 760.
- [5] K. Subramanian and A. Brandenburg 2004. *Nonlinear current helicity fluxes in turbulent dynamos and alpha quenching*, Phys. Rev. Lett. **93**, 205001.
- [6] K. Subramanian and A. Brandenburg 2006. *arXiv: astro-ph/0509392*, Magnetic helicity density and its flux in inhomogeneous turbulence.
- [7] A. S. Brun, M. S. Miesch and J. Toomre 2004. *Global-scale turbulent convection and magnetic dynamo action in the solar envelope*, Astrophys. J. **614**, 1073 – 1098.
- [8] A. A. Schekochihin, N. E. L. Haugen, A. Brandenburg, S. C. Cowley, J. L. Maron and J. C. McWilliams 2005. *Onset of small scale dynamo at small magnetic Prandtl numbers*, Astrophys. J. **625**, L115 – L118.
- [9] A. Brandenburg and G. R. Sarson 2002. *The effect of hyperdiffusivity on turbulent dynamos with helicity*, Phys. Rev. Lett. **88**, 055003.
- [10] N. E. L. Haugen and A. Brandenburg 2006. *arXiv: astro-ph/0412666*, Hydrodynamic and hydromagnetic energy spectra from large eddy simulations.

MHD turbulence in a rotating spherical Couette flow of sodium with an imposed dipolar magnetic field

T. Alboussière, D. Brito, P. Cardin, N. Gagnière, D. Jault, H-C. Nataf and D. Schmitt
*LGIT, CNRS, Observatoire de Grenoble, Université Joseph-Fourier
Maison des Géosciences, BP 53, 38041 Grenoble Cedex 9, FRANCE*

Most planets of the solar system have or have had a self-sustained internal magnetic field. Fluid motions in planetary liquid cores are presumably governed by a balance between rotation and magnetic forces, a regime called magnetostrophic. We have designed an experiment DTS (Derviche Tourneur Sodium) in order to study such a magnetostrophic regime [1].

The experimental set-up is sketched in figure 1: forty litres of liquid sodium fill a spherical shell between a 7.4cm-radius copper inner sphere and a 21-cm radius outer shell made of stainless steel. Both spheres sketched in figure 2 can rotate independently around a vertical axis at different angular frequencies between -30 and 30 Hz. The inner sphere encloses a permanent magnet providing a dipolar field with a moment of 700 Am² (B=0.175 T at the equator of the inner sphere and B=0.008 T at the equator of the outer sphere). The magnetic Reynolds number ranges from 1 to 35.

We have set-up several types of physical measurements in order to characterize the magnetohydrodynamical fluid flow : (i) the velocity and torques delivered by both motors are recorded during the experiments, (ii) the radial and azimuthal components of the sodium velocity are measured by ultrasonic Doppler velocimetry ([2]), (iii) differences in electrical potential are measured at the surface of the external sphere, (iv) the induced magnetic field is measured outside the external sphere (vi) the dynamical pressure is measured at the outer boundary of the fluid flow.

The measurements reveal that the amplitude of the axisymmetric component of the fluid velocity can exceed that of either spheres ([3]). This super-rotation is expected theoretically and in agreement with previous linear numerical modeling ([4], [5]), but we show that non-linear effects modify its characteristics. Both axisymmetric (including realistic boundary conditions and non linear axisymmetric terms) and non-axisymmetric (three-dimensional) numerical simulations of the DTS flow will be compared with the experimental results. Experiments also demonstrate that several solutions for the fluid flow are obtained for a given forcing (fixed inner sphere rotation rate and fixed outer sphere rotation rate); furthermore, spontaneous bifurcations between these different states are also observed during a single run for a given forcing..

We have started the investigation of the instabilities and turbulence that develop in the DTS experiment. Different regions of the experiment are in different dynamical regime: near the inner sphere, magnetic forces dominate, while inertial forces play a strong role near the outer sphere. When the outer sphere is rotating, the Coriolis force inhibits vertical motions and favors azimuthal velocities. We explore the characteristics of waves and turbulence in these different regions. Analysis in time of the differences in electrical potential and induced magnetic field are in particular used to detect the propagation of waves in the DTS flow.

We will discuss the implications of these new measurements for MHD turbulence and dynamo action.

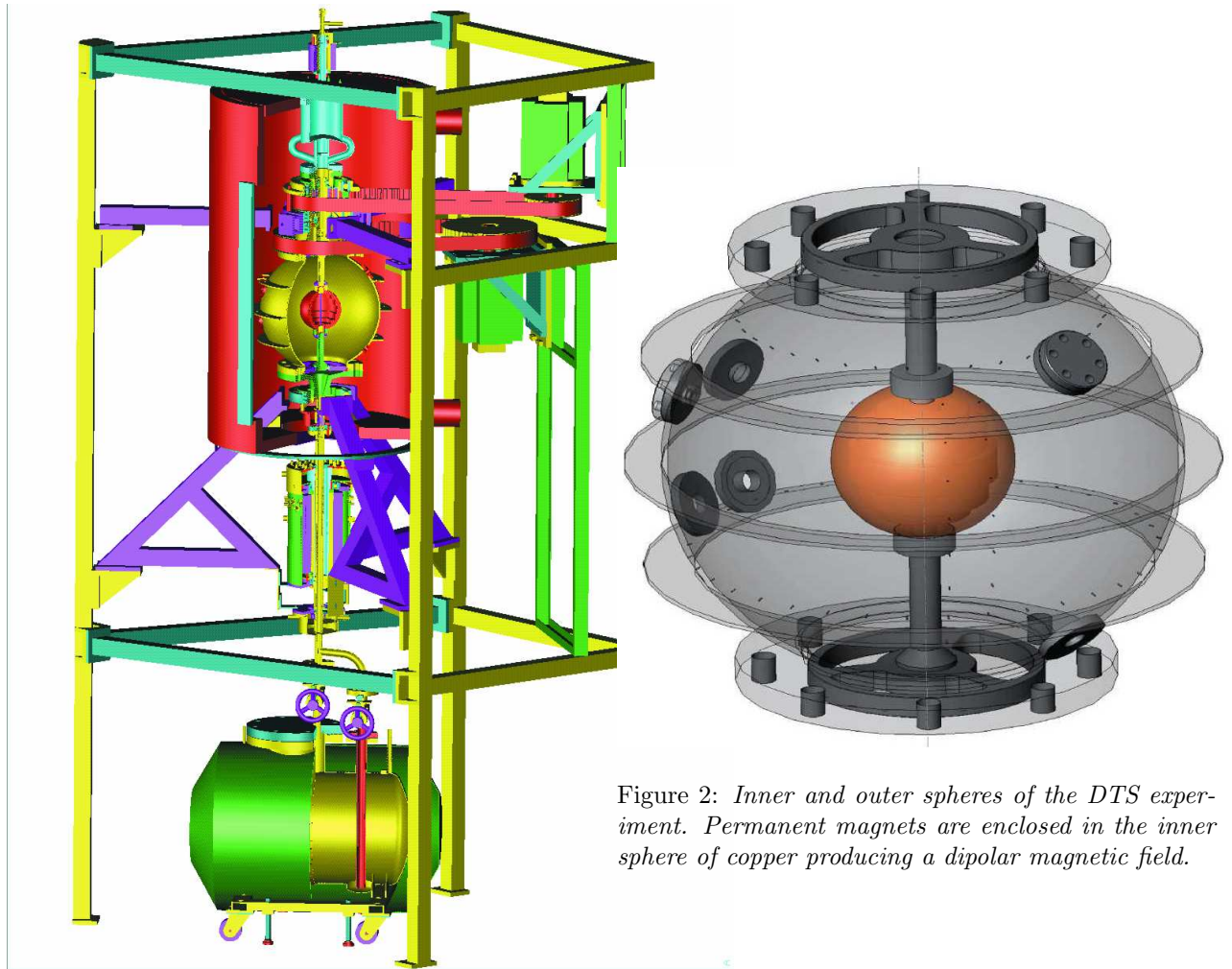


Figure 1: *Sketch of the DTS experiment.*

Figure 2: *Inner and outer spheres of the DTS experiment. Permanent magnets are enclosed in the inner sphere of copper producing a dipolar magnetic field.*

References

- [1] P. Cardin, D. Brito, D. Jault, H.-C. Nataf, J.-P. Masson 2002 *Towards a rapidly rotating liquid sodium dynamo experiment*, *Magneto hydrodynamics*, **38**, 177 – 189.
- [2] D. Brito, H.-C. Nataf, P. Cardin, J. Aubert and J.-P. Masson 2001. *Ultrasonic Doppler velocimetry in liquid gallium*, *Experiments in fluids*, **31**, 653 – 663.
- [3] H. Nataf, H. and Alboussière, T. and Brito, D. and Cardin, P. and Gagniere, D. Jault, J.-P. Masson, N. and Schmitt, D. *Experimental study of super-rotation in a magnetostrophic spherical Couette flow*, In press in *Geophys. Astrophys. Fluid Dyn.*
- [4] E. Dormy, P. Cardin and D. Jault 1998. MHD flow in a slightly differentially rotating spherical shell, with conducting inner core, in a dipolar magnetic field, *Earth and Planetary Science Letters*, **160**, 15–30.
- [5] E. Dormy, D. Jault and A. M. Soward 2002. A super-rotating shear layer in magnetohydrodynamic spherical Couette flow, *J. Fluid Mech.*, **452**, 263–291.

Scaling laws for dynamos in rotating spherical shells and application to planetary magnetic fields

U. R. Christensen,¹ and J. Aubert²

¹*Max-Planck-Institute für Sonnensystemforschung, Katlenburg-Lindau, Germany*

²*Laboratoire de Dynamique des Systemes Geologiques, Institut de Physique du Globe de Paris, France*

We study numerically an extensive set of dynamo models in rotating spherical shells with the geometry of Earth's core, covering a wide range of control parameters. The Ekman number E varies between 10^{-6} and 3×10^{-4} , the magnetic Prandtl number Pm between 0.06 and 10, the Prandtl number Pr between 0.1 and 10, and the Rayleigh number Ra is up to 50 times critical. Convection is driven by a fixed temperature contrast between rigid boundaries. There are two distinct classes of solutions with strong and weak dipole contributions to the magnetic field, respectively. The transition from dipolar to non-dipolar dynamos is found when the scale-dependent Rossby number, $Ro_\ell = U/(\Omega\ell)$, exceeds a value of ≈ 0.12 independent of the values of E , Pr and Pm (U is the rms-velocity, Ω rotation rate, and ℓ a characteristic length scale of the flow). Since Ro_ℓ measures the importance of inertial forces to the Coriolis force, dipolar dynamos break down when inertia starts to play a significant role in the force balance.

We find that in the dipolar regime the minimum magnetic Reynolds number Rm for self-sustained dynamos is independent of the magnetic Prandtl number Pm in the range 40 - 50. However, dynamos at low Pm exist only at sufficiently low Ekman number E . The lowest magnetic Prandtl number at which we find a self-sustained dipolar dynamo varies as $Pm \sim E^{3/4}$. At low Pm the hydrodynamic Reynolds number must be large to exceed the critical value of Rm . The associated inertial effects have an adverse influence on the dynamo and a low Ekman number is required to balance them by strong rotational forces.

For dynamos in the dipolar regime we attempt to establish scaling laws that fit our numerical results. Assuming that diffusive effects do not play a primary role, we introduce non-dimensional parameters that are independent of any diffusivity. As the primary control parameter, we define a modified Rayleigh number based on the advected heat (or buoyancy) flux Q , $Ra_Q^* \sim Q/(\Omega^3 D^4)$, where D is the shell thickness. Ra_Q^* is equivalent to the non-dimensional power generated by buoyancy forces. Characteristic properties of the solution are described by the Rossby number $Ro = U/(\Omega D)$ for the flow velocity, the Lorentz number $Lo = B/([\mu\rho]^{1/2}\Omega D)$ for the magnetic field strength B , and a modified Nusselt number $Nu^* \sim Q/(\Omega\Delta TD^3)$ for the heat transport efficiency. To first approximation, all our dynamo results can be collapsed into simple power-law dependencies on the modified Rayleigh number, with approximate exponents of 2/5, 1/2 and 1/3 for the Rossby number, modified Nusselt number and Lorentz number, respectively. Residual dependencies on the parameters related to diffusion are weak. The Ekman number and hydrodynamic Prandtl number seem to have no effect, but an influence on the magnetic Prandtl number, with a power law exponent of order 1/10, may exist. A similar weak dependency on Pm has been found before in a scaling law for the ohmic dissipation time in numerical dynamo models, but has been rejected because it did not agree well with the ohmic dissipation observed in the Karlsruhe dynamo experiment, where Pm is much smaller than in the models.

The Elsasser number Λ , which is the conventional measure for the ratio of Lorentz force to Coriolis force, is found to vary widely. Our scaling laws are in agreement with the assumption that the magnetic field strength is controlled by the available power and not necessarily by a force balance. In fact, the scaling law for the Lorentz number requires for a good fit the introduction of a correction factor which accounts for the fraction of energy dissipated by viscous rather than by ohmic dissipation. We try to assess the relative

importance of the various forces by studying sources and sinks of enstrophy (vorticity squared). In general Coriolis and buoyancy forces are of the same order, inertia and viscous forces make smaller and variable contributions, and the Lorentz force is highly variable. We can give only a partial theoretical basis for our scaling law. The missing piece is an explanation for the empirical 2/5-exponent in the law for the Rossby number.

We use our scaling law for the Rossby number to deduce the Rayleigh number of the Earth's core. Using core flow velocity estimates obtained from geomagnetic secular variation, we obtain Ra_Q^* to be about 3×10^{-13} and an associated buoyancy flux of 3×10^4 kg/sec. When we assume that this represents predominantly the compositional flux of light element which is rejected when the inner core solidifies, we predict a small growth rate of the inner core of order 0.1 mm/yr and an inner core age of the order 3.5 Gyr.

When we take a power law exponent of 1/3 in the scaling law for the Lorentz number and ignore the possible weak dependence on Pm , a surprising implication is the independence of magnetic field strength B on both the conductivity and the rotation rate. B is basically controlled by the buoyancy flux. For our estimate of the buoyancy flux we obtain a magnetic field strength of order 1 mT inside the core. This is slightly low compared to previous estimates, but is still reasonable and in agreement with a core field estimate from the possible observation of torsional oscillations.

Applying our scaling laws to other planetary dynamos, we find that the observed excess luminosity of Jupiter implies an internal field of 8 mT, in agreement with Jupiter's external field being ten times stronger than that of the Earth. For Saturn the predicted magnetic field seems too strong and Mercury's very weak field cannot be explained by a very low buoyancy flux in the core, because this would correspond to a subcritical magnetic Reynolds number. Possibly Earth and Jupiter fall into the same class of dynamos as are realized in our simulations, whereas different conditions (differential rotation, strongly different inner core size) lead to different dynamos in the other two planets.

Challenges for the future are (1) to establish a more complete theoretical basis for the scaling laws, (2) further explore their range of validity, and (3) to clarify the role of the magnetic Prandtl number. For the latter two points the comparison with future laboratory dynamo experiments will be very helpful.

Global solar dynamo models: application to cyclic photospheric and nearly steady interior fields

Mausumi Dikpati

National Center for Atmospheric Research, 3080 Center Green, Boulder, CO, 80301, USA

The most successful mean-field solar dynamo model is the so-called flux-transport dynamo, which operates with solar-like differential rotation, meridional circulation and α -effect. The Figure below (adopted from [5]) describes how this class of dynamo model works to produce a solar cycle.

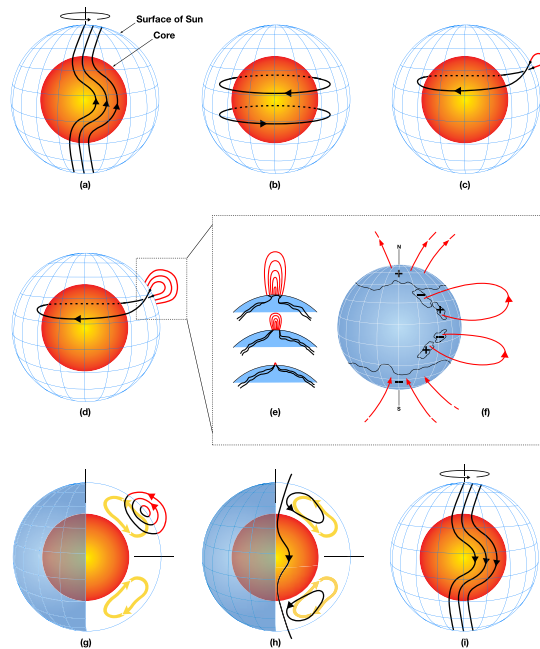


Figure 1: *Schematic of solar flux-transport dynamo processes. Red inner sphere represents the Sun's radiative core and blue mesh the solar surface. In between is the solar convection zone where dynamo resides. (a) Shearing of poloidal field by the Sun's differential rotation near convection zone bottom. The Sun rotates faster at the equator than the pole. (b) Toroidal field produced due to this shearing by differential rotation. (c) When toroidal field is strong enough, buoyant loops rise to the surface, twisting as they rise due to rotational influence. Sunspots (two black dots) are formed from these loops. (d,e,f) Additional flux emerges (d,e) and spreads (f) in latitude and longitude from decaying spots (as described in figure 5 of [1]). (g) Meridional flow (yellow circulation with arrows) carries surface magnetic flux poleward, causing polar fields to reverse. (h) Some of this flux is then transported downward to the bottom and towards the equator. These poloidal fields have sign opposite to those at the beginning of the sequence, in frame (a). (i) This reversed poloidal flux is then sheared again near the bottom by the differential rotation to produce the new toroidal field opposite in sign to that shown in (b).*

In applying flux-transport dynamos to the Sun, we constrain the flow fields by helioseismic measurements. We constrain the least-known ingredient, the diffusivity, by calibrating the model-output with observed magnetic features. We discuss in this talk recent applications of flux-transport dynamos that yield the following major results: (i) a pure interface dynamo without meridional circulation does not work for the Sun; (ii) a cyclic dynamo could be the origin of strong fields in the Sun’s radiative core; (iii) large-scale mean solar cycle features can be predicted.

(i) We [2] show that a pure interface type dynamo will not work for the Sun if the skin effect for poloidal fields does not allow them to penetrate the tachocline. In the absence of tachocline radial shear participating in the dynamo process, a latitudinal differential rotation can provide the necessary Ω -effect to drive an oscillation in an interface dynamo, but it alone cannot produce the latitudinal migration and therefore a reasonable butterfly diagram for the Sun. We show that to make an interface dynamo work with the constraints of interior structure and skin depth, a meridional circulation is essential.

(ii) Any large-scale magnetic fields present in solar/stellar radiative interiors have so far been thought to be primordial or residuals from extinct dynamos. We [3] show that a regular cyclic dynamo can also be the origin of strong magnetic fields in the solar radiative tachocline and interior below. We show that, for a low enough core-diffusivity ($\leq 10^7 \text{ cm}^2 \text{ s}^{-1}$), there exists an oscillatory magnetic field as well as a steady (nonreversing) field of amplitude $\sim 1 \text{ kG} - 3 \times 10^3 \text{ kG}$ or more. The Lorentz force feedback may limit oscillatory dynamo fields to $\sim 30 \text{ kG}$, for which the mean non-reversing toroidal fields is still $\sim 300 \text{ kG}$, for the lowest core diffusivity value. The presence of strong oscillatory and steady toroidal fields in the radiative tachocline implies that there cannot be a slow tachocline; the dynamics should always be fast there, dominated by MHD.

(iii) We [4, 5] construct a dynamo-based tool for predictions of mean solar cycle features by replacing the theoretical Babcock-Leighton type poloidal source with the observed surface magnetic source from decay of active regions. We run the model by assimilating the surface magnetic data since cycle 12, and show that the model can correctly simulate the relative peaks of cycles 16 through 23. The simulations use the first 4 cycles to load the meridional circulation conveyor belt to create the Sun’s memory about its past magnetic fields. Extending the simulation into the future we predict that cycle 24 will be 30-50% stronger than current cycle 23. We show that the key to success of our prediction model lies in the formation of a ‘seed’ for producing cycle n from the combination of latitudinal fields at high latitudes from past three cycles, $n-1$, $n-2$ and $n-3$, instead of just previous cycle’s polar fields, as used in so-called ‘precursor’ prediction methods.

Finally we close by mentioning a few open problems for future research in this field: (i) simulating features in north and south hemispheres separately to look for additional forecast skill, as well as the influence of magnetic links between the two hemispheres, (ii) extension of simulations of relative cycle peaks back to the earliest usable records, starting with cycle 1 around 1750, (iii) additional tuning of the model to improve the skill at predicting two sunspot cycles ahead. Two particularly important generalizations that need to be done are: to include departures from axisymmetry, since many solar cycle features are longitude-dependent, and to include $\mathbf{j} \times \mathbf{B}$ force type feedbacks on the differential rotation and meridional circulation.

References

- [1] H. W. Babcock 1961. *The Topology of the Sun’s Magnetic Field and the 22-YEAR Cycle*, The Astrophysical Journal **133**, 572 – 589.
- [2] M. Dikpati, P. A. Gilman and K. B. MacGregor 2005. *Constraints on the Applicability of an Interface Dynamo to the Sun*, The Astrophysical Journal **631**, 647 – 652.
- [3] M. Dikpati, P. A. Gilman and K. B. MacGregor 2006. *Penetration of Dynamo-generated Magnetic Fields into the Sun’s Radiative Interior*, The Astrophysical Journal **638**, 564 – 575.
- [4] M. Dikpati, G. de Toma and P. A. Gilman 2006. *Predicting the strength of solar cycle 24 using a flux-transport dynamo-based tool*, Geophysical research Letters, **33**, L05102 – L05105.
- [5] M. Dikpati and P. A. Gilman 2006. *Simulating and predicting solar cycles using a flux-transport dynamo*, The Astrophysical Journal, **in press**.

Magnetic turbulence in the Riga Dynamo experiment

Agris Gailitis,¹ Olgerts Lielausis,¹ Ernests Platacis,¹ Gunter Gerbeth,² and Frank Stefani ²

¹*Institute of Physics University of Latvia, LV-2169 Salaspils, Latvia*

²*Forschungszentrum Rossendorf, PO Box 510119, 01314, Dresden, Germany*

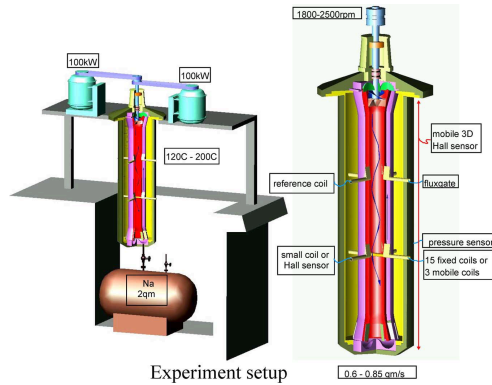


Figure 1: *Experiment setup*

Riga dynamo experiment demonstrates that enough strong and appropriately directed flow of fluid electroconductor generates magnetic field very likely as Earth and other celestial bodies do. Two 100 kW motors (Fig. 1) are driving propeller which forces molten sodium to circulate inside an annular vessel, part of which is located in the basement of sodium lab. The sodium flow is directed by two thin coaxial electro-conducting cylindrical partition walls. In the central channel sodium is swirling down from the propeller. In the coaxial counter-flow channel the flow is raising straight up to the propeller. In an outer part of the vessel the sodium is move-less, it serves for electrical connection. Depending on sodium temperature at a propeller speed of

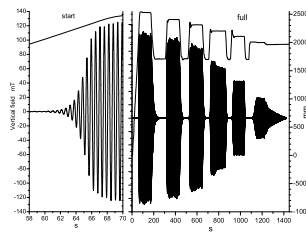


Figure 2: *Field record*

1800 – 2000 rpm (flow-rate about 0.6 qm/s) the zero state for magnetic field is becoming unstable and field appears seeming from nothing (Fig.2,). Magnetic field values are recovered from coil voltage records by means of Fast Fourier processing.

For finer spectral resolution two small coils were inserted alternately in a narrow channel tip penetrating deep inside the central flow. Examples for recorded signals and Fourier processed fields are on Fig.3 while power spectra on Fig.4 .

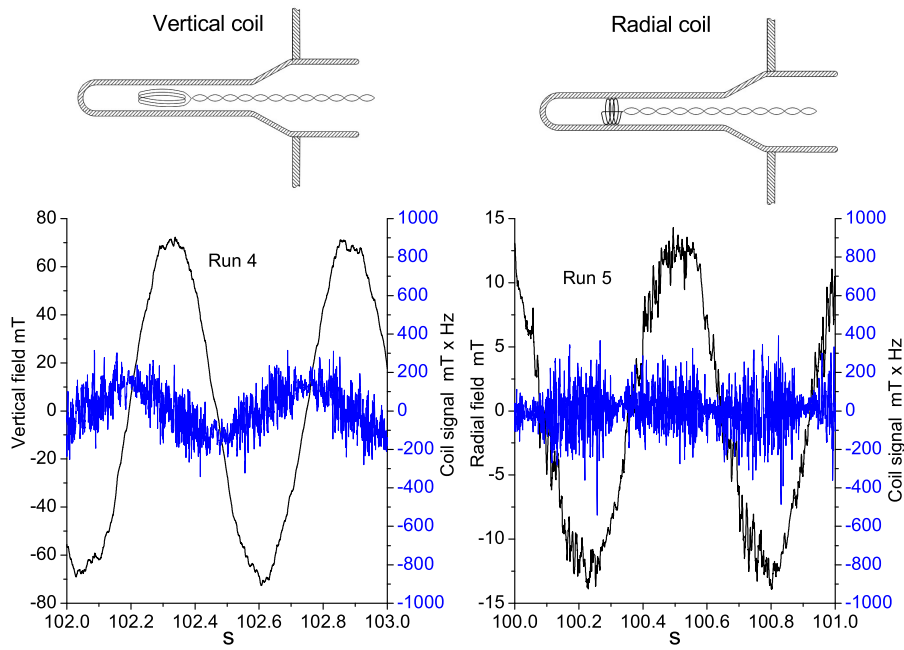


Figure 3: *Examples of recorded signals and Fourier processed field*

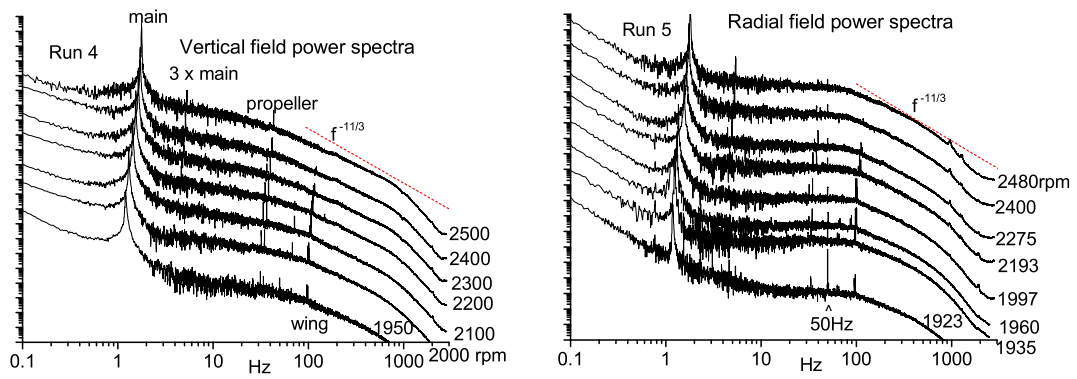


Figure 4: *Magnetic spectra*

Experimental and numerical studies of the role of turbulence on current generation and magnetic field self-excitation in the Madison Dynamo Experiment

Cary Forest,¹ Adam Bayliss,¹ Mark Nornberg¹ and Erik Spence¹

¹University of Wisconsin, Madison, Wisconsin, 53711 USA

The Madison Dynamo experiment is investigating the role of turbulence on current generation and self-excitation of magnetic fields. The geometry, a 1 meter diameter spherical vessel with a flow driven by two counter rotating internal impellers, is motivated to a large degree by the two vortex flow proposed by Dudley and James. The geometry is shown in Fig. 1. In this talk will report on an effort to compare the results from the experiment with simulations of a similar geometry using a 3D numerical solution of the MHD equations.

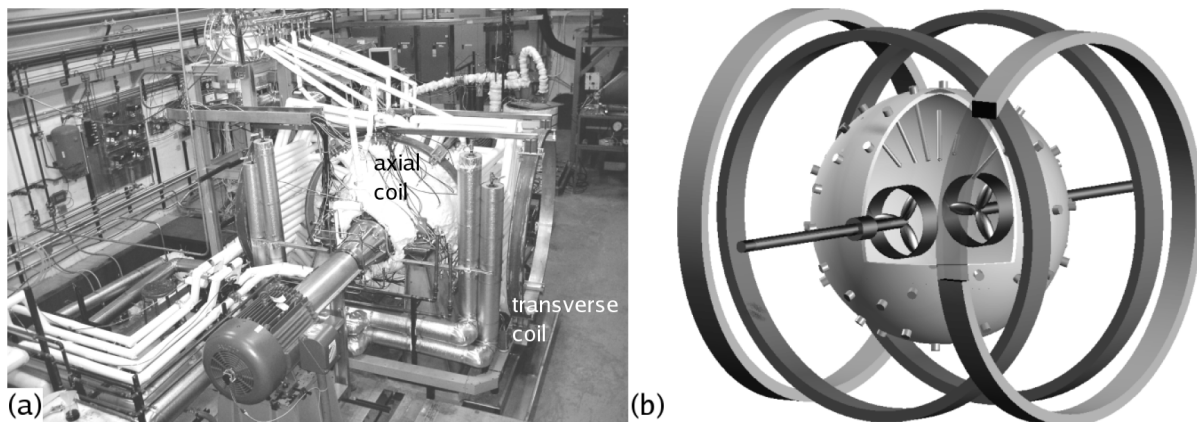


Figure 1: Photograph and schematic of the Madison Dynamo Experiment. The sphere is 1 meter in diameter. It is filled with 105–110°C liquid sodium and a flow is created by two counter-rotating impellers. Two sets of coils, one coaxial with and one transverse to the drive shafts, are used to apply various magnetic field configurations. The magnetic field induced by the flow is measured using Hall-effect sensors both on the surface of the sphere and within tubes that extend into the flow.

The numerical model is a pseudo-spectral code using spherical harmonic basis functions in the azimuthal and polar directions and finite difference in the radial direction. An Adams-Bashforth predictor corrector technique for the advancement of the non-linear terms. A simple impeller model has been developed which drives a flow quantitatively similar to that observed in water experiments (in a geometry f dimensionally identical to the sodium experiment). These flows can be dynamos, depending upon the value of the magnetic Reynolds number $Rm = \mu_0 \sigma Va$ and the fluid Reynolds number $Re = Va/\nu$ of the flow. For $Re < 420$ the flow is laminar and the dynamo transition is governed by a simple threshold in $Rm > 100$, above which a growing magnetic eigenmode is observed that is primarily of a dipole field transverse to axis of symmetry of the flow. In saturation the Lorentz force slows the flow such that the magnetic eigenmode becomes marginally stable. For $Re > 420$ and $Rm \sim 100$ the flow becomes turbulent and the dynamo eigenmode is suppressed. The mechanism of suppression is due to a combination of a time varying large-scale field and the presence

of fluctuation driven currents (such as those predicted by the mean-field theory) which effectively enhance the magnetic diffusivity. For higher Rm a dynamo reappears, however the structure of the magnetic field is often different from the laminar dynamo; it is dominated by a dipolar magnetic field aligned with the axis of symmetry of the mean-flow which is apparently generated by fluctuation-driven currents.

In the experiment, a fully self-sustained dynamo has not yet been observed, although there is evidence for an intermittently excited magnetic field which has structure similar. There may be evidence for intermittent self-excitation in the simulations, but the limited duration of the runs makes it difficult to determine this for certain.

The experiments have been focused on understanding the magnetic fields generated by the turbulent flows when a weak seed field is applied which shares a symmetry axis with the mean flow. Clear evidence for the presence of fluctuation driven currents is present. The EMF generated by the mean-flow and mean-magnetic field lead to currents which are unable to account for the detailed structure of the mean-magnetic field. In the experiment, there is a dipole observed in the experiment which cannot be explained by the axisymmetric mean flows, and the magnitude of the predicted fields are much larger than those observed. Similar behavior is also seen in numerical simulations of turbulent flows (subcritical for dynamo excitation) with externally applied magnetic fields.

Finally, the spectrum of the velocity field and magnetic field fluctuations are discussed. In the experiment, clear evidence for an inertial range and a dissipation scale are observed on single point measurements of the magnetic field using a hall probe and of the velocity field using LDV in the water experiment. The dissipation scale for the magnetic field moves to higher frequencies as Rm is increased. Simulations at $Re \sim 1000$ predict qualitatively similar behavior.

References

- [1] M. Nornberg, E. Spence, R. Kendrick, C. Jacobson, and C. Forest, *Phys. Plasmas* **13**, 055901 (2006).
- [2] E. Spence, M. Nornberg, C. Jacobson, R. Kendrick, and C. Forest, *Phys. Rev. Lett.* **96** 055002 (2006).
- [3] M. Nornberg, C. Jacobson, E. Spence,, R. Kendrick, and C. Forest, to be published in *Phys. Rev. Lett.* (2006).
- [4] R.A. Bayliss, M. Nornberg, P. Terry and C. Forest, submitted to *Phys. Rev. E* (2006).

Rapidly Rotating Convection and the Geodynamo

Chris Jones

University of Leeds, LS2 9JT, UK

Rapidly rotating convection in spherical geometry has been explored using the quasi-geostrophic approximation [1]. This is a reasonable model of convection between rotating spherical shells outside the tangent cylinder that touches the inner core. This approximation assumes a simple z -dependence and solves the two-dimensional nonlinear fluid equations in s , the distance from the axis, ϕ the azimuthal coordinate, and time t . Attention is focussed on the heat transport and the azimuthal zonal flow. We find that the local Peclet number, the product of the typical convective velocity and local convective length scale divided by the thermal diffusivity, is helpful for understanding the dynamics of rapidly rotating convection.

For small $R/R_c - 1$, R being the Rayleigh number and R_c its linear critical value, the Nusselt number varies linearly with $R/R_c - 1$, with a slope that diminishes rapidly as the Prandtl number $P = \nu/\kappa \rightarrow 0$. At larger values of $R/R_c - 1$ the Nusselt number becomes less dependent on P , and eventually increases more slowly with $R/R_c - 1$ as thin thermal boundary layers develop. At small $R/R_c - 1$, the zonal flow $U_\phi^0 \sim \hat{U}_c^2$, where \hat{U}_c is the convective velocity, but as $R/R_c - 1$ increases saturation occurs and the exponent is reduced to $U_\phi^0 \sim \hat{U}_c^{4/3}$ approximately. Some possible reasons for this exponent will be discussed. The zonal flow sometimes exhibits a multiple jet structure, and sometimes has a simple radial structure. Factors affecting multiple jet formation will be considered.

We compare our results with the inertial scaling, [2, 3], developed to study rapidly rotating convection, which predicts that $\hat{U}_c \sim R_Q^{2/5}(EP)^{1/5}$, where R_Q is the flux Rayleigh number, $R_Q = R(Nu - 1)$, and E is the Ekman number, $\nu/\Omega d^2$, d being the gap between the inner and outer core. The scalings for R_Q and E are in reasonable agreement with our numerical solutions, but the Prandtl number scaling is poor. It appears that the viscous length scale at onset, $dE^{1/3}$, is still relevant even at Rayleigh numbers 50 times critical.

When a dynamo generated magnetic field is present, Christensen and Aubert [4] find that the scaling $\hat{U}_c \sim R_Q^{2/5}$ still holds (the Rayleigh number here being defined in terms of the rotation time rather than the dissipation time), while Starchenko and Jones [5] argued that $\hat{U}_c \sim R_Q^{1/2}$. In the Earth's core, velocities are so low that inertia is negligible except on very small length scales. The conditions that inertia is negligible in spherical dynamo models have been investigated recently by Sreenivasan and Jones [6].

The vorticity equation can be written

$$-2(\boldsymbol{\Omega} \cdot \nabla)\mathbf{u} = \nabla \times g\alpha T \hat{\mathbf{r}} + \frac{1}{\rho} \nabla \times (\mathbf{j} \times \mathbf{B}), \quad (1)$$

suggesting $2\Omega \hat{U}_c / L_z \sim g\alpha T / L_x$. The temperature perturbation T can be eliminated using the convective heat flux per square metre $F \sim \rho c_p \hat{U}_c T$, to give

$$\hat{U}_c \sim \left(\frac{g\alpha F}{\rho c_p \Omega} \right)^{1/2} \frac{L_z}{2L_x}, \quad (2)$$

or $\hat{U}_c \sim R_Q^{1/2}$ if the ratio L_z/L_x is constant. It is therefore the asymptotic behaviour of L_z/L_x which is crucial. In the presence of a magnetic field, the zonal flow is much reduced, and more interest attaches to the strength of the generated magnetic field. Ohmic dissipation balances the buoyancy work, since viscous dissipation is small, so

$$\eta \mu \mathbf{j}^2 \sim \frac{g\alpha F}{c_p}. \quad (3)$$

The length scale δ_B over which the magnetic field varies comes from the induction equation

$$(\mathbf{B} \cdot \nabla)\mathbf{u} \sim \eta \nabla^2 \mathbf{B} \rightarrow \delta_B \sim Rm^{-1/2} d \quad (4)$$

if flux ropes with thickness δ_B are created, [7]. Then setting $|\mu\mathbf{j}| \sim |\mathbf{B}|/\delta_B$ and using (3),

$$B \sim \mu^{1/2} d^{1/2} \left(\frac{g\alpha F}{c_p} \right)^{1/2} \frac{1}{\hat{U}_c^{1/2}}. \quad (5)$$

The scaling for \hat{U}_c , (2), can then be used to estimate the typical field strength. This field strength scaling implies that the Lorentz force is primarily balanced by pressure in the flux ropes where it is created. To obtain the magnetic field strength directly from the vorticity equation (1) we must note that in the magnetic flux tube configuration the current varies only slowly along the (long) flux tube.

These scalings can be applied to obtain estimates of the typical velocity and magnetic field strength of the planets. For a planet to actually have an active dynamo obeying these scalings, the total heat flux must exceed the heat flux that can be conducted down the adiabat at least somewhere in the core. Also, the magnetic Reynolds number predicted by (2) must be sufficient for dynamo action to occur.

References

- [1] N. Gillet and C.A. Jones 2006. *The quasi-geostrophic model for rapidly rotating spherical convection outside the tangent cylinder*, Journal of Fluid Mechanics, **554**, 343 – 369.
- [2] A.P. Ingersoll and D. Pollard 1982. *Motions in the interiors and atmospheres of Jupiter and Saturn: scale analysis, anelastic equations, barotropic stability criterion*. Icarus, **52**, 62 – 80.
- [3] J. Aubert, D. Brito, H-C Nataf, P. Cardin and J.P. Masson 2001. *A systematic experimental study of spherical shell convection in water and liquid gallium*. Physics of the Earth and Planetary Interiors, **128**, 51 – 74.
- [4] U.R. Christensen and J. Aubert 2006. *Scaling properties of convection-driven dynamos in rotating spherical shells and application to planetary dynamos*. To appear in Geophysical Journal International.
- [5] S. Starchenko and C.A. Jones 2002. *Typical velocities and magnetic field strengths in planetary interiors*. Icarus, **157**, 426 – 435.
- [6] B. Sreenivasan and C.A. Jones 2006. *The role of inertia in the evolution of spherical dynamos*. Geophysical Journal International, **164**, 467 – 476.
- [7] D.J. Galloway, M.R.E. Proctor and N.O. Weiss 1978. *Magnetic flux ropes and convection*. Journal of Fluid Mechanics, **87**, 243 – 261.

GTP Workshop on
**Modeling MHD Turbulence; Applications to
Planetary and Stellar dynamos**
at NCAR, 27-30 June, 2006, Boulder, CO, USA

Building laboratory models of planetary cores

Daniel P. Lathrop

Department of Physics, University of Maryland, College Park, MD

We probe aspects of the dynamics of fluid flows in planetary cores using experiments in liquid sodium, liquid helium, liquid nitrogen or water (not of course mixed together!). Key to these several experimental devices is exploring how turbulence is effected by rotation, magnetic fields or both. As both add some measure of elasticity to the flows, several types of oscillatory behavior are observed depending on the force balances involved. Ordering the Coriolis, Lorentz, and Inertial forces is key to understanding the complicated states observed. While these experiments are undertaken in part to understand the geodynamo, they have led to a number of different first observations, including the magnetorotational instability, and inertial waves in both spherical Couette flow and decaying turbulence in cryogenic flows. These different approaches to using laboratory experiments are opening up a new direction to understanding the dynamics of the Earth's outer core and other Planetary interiors.

Lagrangian evolution, non-Gaussianity, and statistical geometry in intermittent hydrodynamic turbulence

Charles Meneveau¹, Yi Li¹, Laurent Chevillard¹ and Carlos Rosales¹

*¹Department of Mechanical Engineering and Center for Environmental and Applied Fluid Dynamics
Johns Hopkins University, Baltimore MD 21218, USA*

Recent theoretical and numerical results on intermittency in hydrodynamic turbulence and scalar transport are described, with special emphasis on the Lagrangian evolution. First, we derive the advected delta-vee system. This simple dynamical system deals with the Lagrangian evolution of two-point velocity and scalar increments in turbulence [1, 2]. It shows that ubiquitous trends of three-dimensional turbulence such as exponential or stretched exponential tails in the probability density functions of transverse velocity increments, as well as negatively skewed longitudinal velocity increments, emerge quite rapidly and naturally from initially Gaussian ensembles. Further extensions of the system are shown to provide simple explanations for other known intermittency trends in turbulence: (i) that transverse velocity increments tend to be more intermittent than longitudinal ones, (ii) that in two dimensions, vorticity increments are intermittent while velocity increments are not, (iii) that scalar increments typically become more intermittent than velocity increments and, finally, (iv) that velocity increments in four-dimensional turbulence are more intermittent than in three dimensions. While the origin of these important trends can thus be elucidated qualitatively, predicting quantitatively the statistically steady-state levels and dependence on scale remains an open problem that would require including the neglected effects of pressure, inter-scale interactions and viscosity.

Next, we describe recent efforts to incorporate a new model for the anisotropic part of the pressure Hessian into the Lagrangian dynamics. A stochastic model for the full velocity gradient tensor is proposed, based on a closure in which spatial gradients of pressure and the viscous Laplacian term are expressed in terms of the material deformation tensor (this is also related to the tetrad model of Ref. [4]). Here the deformation tensor is modeled based on the assumption that the velocity gradient tensor's autocorrelation along its Lagrangian history is strong over a Kolmogorov time-scale, and is uncorrelated for longer times[3]. The model reproduces important geometric trends such as vorticity-strain rate alignments, joint PDFs in the so-called "R-Q" plane, as well as nearly lognormal statistics for the dissipation rate.

Finally, we describe the implications of these findings on the problem of generating synthetic 3D vector fields that mimic non-Gaussian turbulence statistics, and that may be used as initial or inlet boundary conditions for simulations. Inspired by the advected delta-vee system, a simple method is proposed based on the minimal Lagrangian map, by which an initial Gaussian field generated using random-phase Fourier modes is deformed[5]. The deformation is achieved by moving fluid particles of a sequence of low-pass filtered fields at their fixed velocity for some scale-dependent time-interval, interpolating onto a regular grid, and imposing the divergence-free condition. Statistical analysis shows that the resultant non-Gaussian field displays many properties commonly observed in turbulence, ranging from skewed and intermittent velocity gradient and increment probability distributions, preferential alignment of vorticity with intermediate strain-rate, and non-trivial vortex stretching statistics. Differences begin to appear only when interrogating the data with measures associated with intense vortex tubes that are conspicuously absent in the synthetic field. To explore the dynamical implications of these observations, the synthetic non-Gaussian fields are used as initial conditions in DNS and LES of decaying isotropic turbulence, and results are compared with initializations using Gaussian fields. The non-Gaussian synthetic fields yield more realistic results with

significantly shortened initial adjustment periods.

Acknowledgments

The authors gratefully acknowledge the support from the National Science Foundation (grant ITR-0428325) and the Keck Foundation Postdoctoral Fellowship program. CR also thanks the financial support from the MECESUP Program FSM0104 (Universidad Técnica Federico Santa María, Chile).

References

- [1] Li, Y. & Meneveau, C. 2005. *Origin of non-Gaussian statistics in hydrodynamic turbulence*. Phys. Rev. Lett. **95**, 164502.
- [2] Li, Y. & Meneveau, C. 2006. *Intermittency trends and Lagrangian evolution of non-Gaussian statistics in turbulent flow and scalar transport*. J. Fluid Mech., in press.
- [3] Chevillard, L. & Meneveau, C. 2006. *Lagrangian dynamics of the velocity gradient tensor: a stochastic model*, in preparation.
- [4] Chertkov, M., Pumir, A. & Shraiman, B. I. 1999. *Lagrangian tetrad dynamics and the phenomenology of turbulence*. Phys. Fluids **11**, 2394–2410.
- [5] Rosales, C. & Meneveau, C. 2006. *A minimal multiscale Lagrangian map approach to synthesize non-Gaussian turbulent vector fields*. Phys. Fluids, submitted.

Magnetic dynamo calculations inside a sphere

David C. Montgomery

*Department of Physics and Astronomy, Dartmouth College, Hanover, NH 03755 and
National Center for Atmospheric Research, P.O. Box 3000, Boulder, CO, 80307-3000*

This presentation describes some recent computational efforts to demonstrate magnetic dynamo action inside a sphere that is filled with an incompressible electrically conducting fluid, avoiding rectangular periodic boundary conditions. The motivation is ultimately directed toward planetary and laboratory dynamos, but our first concern is to identify and understand the physical processes involved at the simplest level consistent with the magnetohydrodynamic (MHD) equations. The idea is to compute the simplest dynamo situations first, and put in the imaginable complications (thermal convection, irregularities on the inner surface of the Earth's mantle, variable fluid mass density, a differentially rotating inner core, for examples) one at a time. We are not putting a high priority on realistic numbers at this point.

The system studied is a sphere with a weightless, rigid, perfectly conducting shell at a radius $r = R$. The shell is assumed to be coated on the inside with a very thin layer of insulating dielectric, so that the normal components of the magnetic field and current density vanish there. The normal components of the velocity field and vorticity are also assumed to vanish at $r = R$. These conditions are implied by, but do not imply, no-slip boundary conditions on the velocity field. In addition to being difficult to implement, there are conceptual difficulties associated with no-slip boundary conditions that remain unresolved (e.g., [1] and [2]) and controversial, and are better engaged with in simpler situations than this one.

Inside the sphere, $r < R$, the equations of viscous, resistive, incompressible MHD are assumed to govern the dynamics. We have chosen the sphere to be either stationary or rotating with a constant angular velocity in the latter case by introducing Coriolis and centrifugal terms into the equation of motion. In the induction equation for the magnetic field, no corrections for the fact that the coordinate frame may be rotating and non-inertial are deemed necessary, since the rotation velocity is very small compared to the speed of light.

The method of solution is wholly spectral; all of the solenoidal fields are expanded as series of Chandrasekhar-Kendall (C-K) orthonormal eigenfunctions of the curl. A similar program was used some years ago in cylindrical geometry [3] for nonlinear MHD computations. The C-K functions are believed to be complete for solenoidal fields, but a proof has been given only for the cylindrical case [4]. The boundary conditions are all built into the expansion functions themselves, and do not require attention again in the computation. The dynamical variables are the time-dependent complex coefficients in the expansions, which are advanced by a set of nonlinear ordinary differential equations. The known quadratic ideal invariants are very well conserved over many eddy-turnover times, for the initial-value problem with zero viscosity and resistivity. We return to configuration space only for graphical purposes. The price paid for this scheme is the absence of fast transforms that make pseudospectral computation in periodic boundary conditions economical, so that the convolution sums become unwieldy at resolutions achievable by FFT-based codes. The advantages are that the boundary conditions are automatically satisfied and the expansion functions are physically natural to the geometry: far fewer of them are necessary to represent the MHD structures that arise than would be necessary, for example, in a rectangular Fourier series representation.

Mechanical forcing is introduced as an inhomogeneous term on the right hand side of the equation of motion. The forcing, too, is represented in terms of C-K functions and can be chosen to mimic such processes as thermal convection or irregular boundaries on the inner surface.

The code can be run, of course, as a purely hydrodynamic code by deleting the magnetic terms. Doing so reveals, for the rotating case, flow patterns characteristic of Ekman pumping and internal wave motion in

which the inertial terms in the equation of motion are not neglected and no geostrophic approximations are made. Wide variations in behavior are observed depending upon Rossby number, Reynolds number, Ekman number, and the scale of the forcing terms. Fully exploring the possible parameter space will be a lengthy task. Each corner of parameter space shows its own peculiarities.

Dynamo actions with and without rotation are very different. In both cases, the technique is to force a mechanical flow pattern which may be time dependent but which has ceased to evolve systematically and may or may not be turbulent. Then a small seed magnetic field is introduced and allowed to evolve according to the full set of MHD equations. At the early stages, the magnetic energy is observed either to amplify or decay, and at this stage we may be considered to be solving the kinematic dynamo problem. For the case of amplifying magnetic fields, they may be followed on into the saturation regime, where the Lorentz force is no longer negligible in the equation of motion. Both laminar and disordered magnetic fields can be observed in different parameter regimes, and magnetic dipole moments may be computed. For the former, flips from one dipolar orientation to another are observed in some cases. For the latter, essentially stochastically varying small-scale magnetic fields are possible. Some details appear in Ref. [5].

Future plans involve the inclusion of a differentially rotating inner solid core, and the replacement of the conducting shell by a mechanically impenetrable insulator, so that the generated magnetic field can penetrate the vacuum region outside.

The computations reported here have all been carried out by Dr. Pablo Mininni. The author also wishes to thank Dr. Annick Pouquet for stimulating discussions. This work was supported in part by National Science Foundation Grants ATM-0327533 at Dartmouth and CMG-0327888 at NCAR.

References

- [1] G. Gallavotti 2002. *Foundations of Fluid Dynamics*, (New York: Springer).
- [2] B. T. Kress and D. C. Montgomery 2000. *Pressure determinations for incompressible fluids and magnetofluids*, J. Plasma Physics, **64**, 371 – 377.
- [3] X Shan, et al. Phys. Rev. **44A.**, 6800 (1991); Plasma Phys. and Contr. Fusion **35**, 619 and 1019 (1993).
- [4] Z. Yoshida 1992 *Eigenfunction expansions associated with the curl derivatives in cylindrical geometries: Completeness of ChandrasekharKendall eigenfunctions* J. Math. Phys., **33**, 1252 – 1271.
- [5] P. D. Mininni and D. C. Montgomery 2006. *Magnetohydrodynamic activity inside a sphere*, submitted to Phys. Fluids, arXiv:physics/0602147 (this reference contains a much more extensive bibliography).

Induction measurements in the VKS2 experiment

Romain Volk, Philippe Odier, Jean-François Pinton (1)

Michael Berhanu, Stephan Fauve, Nicolas Mordant, François Pétrélis (2)

Florent Ravelet, Romain Monchaud, Arnaud Chiffaudel, François Daviaud (3)

(1) *Laboratoire de Physique de l'École Normale Supérieure de Lyon, France*

(2) *Laboratoire de Physique Statistique de l'École Normale Supérieure de Paris, France*

(3) *Service de Physique de l'Etat Condensé, Direction des Sciences de la Matière, CEA-Saclay, France*

Abstract We report recent results from the VKS2 experiment: response to an externally imposed homogeneous magnetic field, and transport of a localized applied field.

The VKS2 experiment The VKS project in Cadarache [1] is one of several experiments dedicated to the study of the dynamo effect in an unconstrained homogeneous flows of liquid metals [2]. The acronym “VKS” stands for “von Kármán sodium” and refers to the flow generated between two counterrotating impellers in a finite cylinder. The phenomenology of the time-averaged flow is as follows. Each impeller acts as a centrifugal pump: the fluid rotates with the impeller and is expelled radially. To ensure mass conservation the fluid is pumped in the center of the impeller and recirculates near the cylinder wall. In the exact counter-rotating regime, the mean flow is divided into two toric cells separated by an azimuthal shear layer. The kinetic Reynolds number is about 10^7 and the shear layer instability is a strong source of turbulence. The VKS2 evolution result from flow optimization and numerical inspection of its dynamo behavior [3]. With respect to the first version (VKS1[1]), the motor power has been increased to 300kW and the volume of the conducting domain is twice greater. A temperature regulation allows long measurements in stationary regime. Magnetic Reynolds number between 12 and 50 are reached.

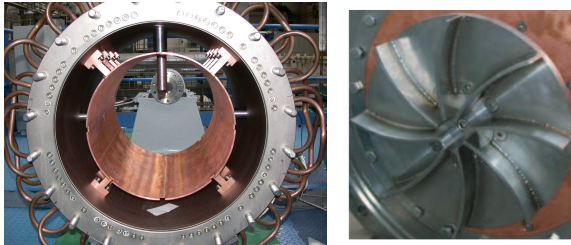


Figure 1: *VKS2 flow vessel and driving impellers*

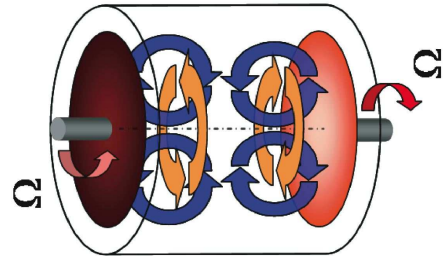


Figure 2: *Mean flow geometry*

Response to a uniform applied field [4] We apply a large scale field with a pair of coils ($B_{0y} = 2.7G$, too weak to modify the flow) in a direction transverse to the axis of rotation of the driving impellers – the direction expected for the dynamo neutral mode in the kinematic dynamo simulations [3]. Fig. 3 shows the evolution of the mean of the induced field b_y in the direction of the applied field. Once $R_m > 20$, $\langle b_y \rangle$ exceeds B_{0y} . In addition, the fluctuations of the induced component b_y are non-Gaussian, – Fig. 4 – at all R_m values. These features are in contrast with VKS1 measurements, where the induced field b_y saturated at $0.4B_{0y}$, and its fluctuations were Gaussian. However, no self-sustained dynamo regime has been reached, and at the largest R_m values we have measured a linear growth of the mean and *rms* values of the induced field. Note, in Fig. 3, that the measured mean values of induction deviate significantly from the ones predicted by induction from the mean flow velocity.

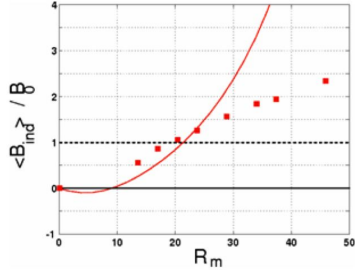


Figure 3: *Evolution of the mean induced field b_y . Solid line: numerical prediction from the mean flow.*

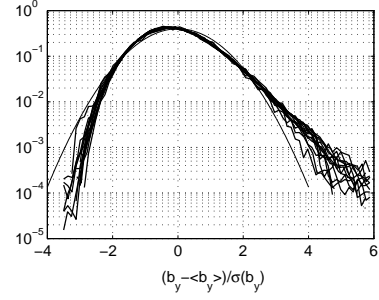


Figure 4: *Corresponding probability density functions of the fluctuations of b_y , comparison to a Gaussian*

Response to a localized applied field [5] We have studied the response when a localized field $\vec{B}_0(\vec{r})$, generated by a NdFeB cylindrical magnet, 22 mm in diameter and 10 mm in height, set within the flow vessel. The maximum value of the field created by the magnet in its vicinity is about 500 G but decays to less than 1 G, at a distance 100 mm away from the magnet. The time recordings of the fluctuations of the three components of the induced magnetic field \vec{B} measured by the probe 200 mm away from the magnet, are displayed in Fig. 5 for $R_m = 30$. We observe an intermittent signal with the occurrence of bursts of magnetic field. The corresponding probability density functions (PDF) are shown in Fig. 6.

These observations are of interest for the analysis of the transport of a magnetic field by turbulence. Indeed, magnetic eigenmodes generated by dynamo mechanisms are usually strongly localized in space. Geophysical or astrophysical flows generally involve regions of strong differential rotation or strong helicity which are not located in the same part of the flow but are both believed to be necessary for dynamo action. It is thus important to understand how the magnetic field induced in one region is transported to the other by strongly turbulent flows.

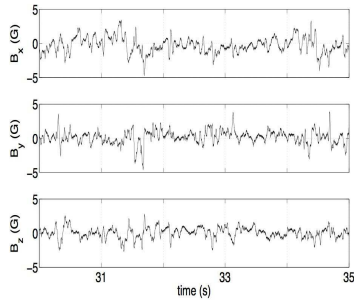


Figure 5: *Transport of a localized applied field: time evolution, at $R_m = 30$.*

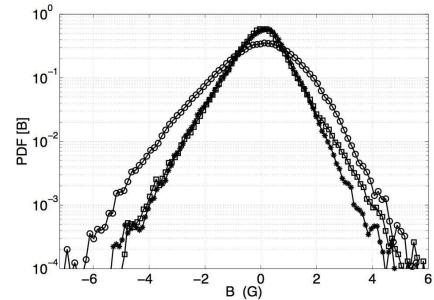


Figure 6: *Corresponding PDFs. B_x (circles), B_y (squares), B_z (ast).*

References

- [1] M. Bourgoin et al. 2002, Phys. Fluids, **14**, 2046.
- [2] A. Gailitis, O. Lielausis, E. Platācis, G. Gerbeth, F. Stefani 2002, Rev. Mod. Phys., **74**, 973.
- [3] F. Ravelet, A. Chiffaudel, F. Daviaud and J. L  orat 2005, Phys. Fluids, **17**, 117104.
- [4] F. Ravelet et al. 2006, *Large and slow fluctuations of level and orientation of induced magnetic field in a turbulent flow of liquid sodium*, Phys. Rev. Lett., submitted.
- [5] R. Volk et al. 2006, *Transport of magnetic field by a turbulent flow of liquid sodium*, Phys. Rev. Lett., to appear.

Linear regime of dynamo action at low magnetic Prandtl number: Role of the mean flow and the velocity fluctuations.

Y. Ponty ¹, P.D. Mininni ², F. Plunian ³, J.-F. Pinton ⁴, H. Politano ¹ and A. Pouquet ².

¹ CNRS UMR6202, Laboratoire Cassiopée, Observatoire de la Côte d'Azur,
BP 4229, Nice Cedex 04, France.

² National Center for Atmospheric Research, P.O. Box 3000, Boulder, CO, 80307-3000, USA.

³ Laboratoires des Écoulements Géophysiques et Industriels,
Boîte Postale 53, 38041 Grenoble Cedex 9, France.

⁴ CNRS UMR5672, Laboratoire de Physique, École Normale Supérieure de Lyon,
46 Allé d'Italie, 69007 Lyon, France.

First, we consider the induction of magnetic field in flows of electrically conducting fluid at low magnetic Prandtl number and large kinetic Reynolds number. Using the separation between the magnetic and kinetic diffusive length scales, we study the response of a forced flow to an externally applied field : topology of the mean induction and time fluctuations at fixed locations. The results are in remarkable agreement with existing experimental data; a global $1/f$ behavior at long times is also evidenced [1].

Secondly, we present a numerical approach to the dynamo problem at low magnetic Prandtl number for different forcing [2, 3, 5]. The difficulty of resolving a large range of scales is circumvented by combining direct numerical simulations, and sub-grid model. Our main findings are that dynamos are observed at low magnetic Prandtl number, few order of magnitude smaller as previous numerical studies and the role of the time average flow on the dynamo onset, compared with the fully turbulent dynamo regime [4]. The competition between the average in time velocity kinematic dynamo modes (Figure 1) and the large scale velocity fluctuation dynamo modes are also investigated.

References

- [1] Y. Ponty, H. Politano & J-F Pinton "Simulation of Induction at Low Magnetic Prandtl Number" *Phys. Rev. Lett.* **92**, pp 144503 (2004).
- [2] Y. Ponty , P. Minnini , A. Pouquet , H. Politano , D. Montgomery , J.-F. Pinton "Numerical study of dynamo action at low magnetic Prandtl numbers" *Phys. Rev. Lett.* **94** , 164502 (2005).
- [3] P. D. Mininni, Y. Ponty, D. C. Montgomery, J-F Pinton, H. Politano, and A. Pouquet "Dynamo Regimes with a Non-helical Forcing" *The Astrophysical Journal*, **626**: 853 -863 (2005)
- [4] Y. Ponty, P.D. Minnini, J.-F. Pinton, H. Politano, A. Pouquet : "Dynamo action at low magnetic Prandtl numbers: mean flow vs. fully turbulent motion", submitted (2006).
- [5] Y. Ponty & F. Plunian "Large scale Dynamo at low magnetic Prandtl number" in preparation.
- [6] VAPOR/NCAR Software : <http://www.vapor.ucar.edu>

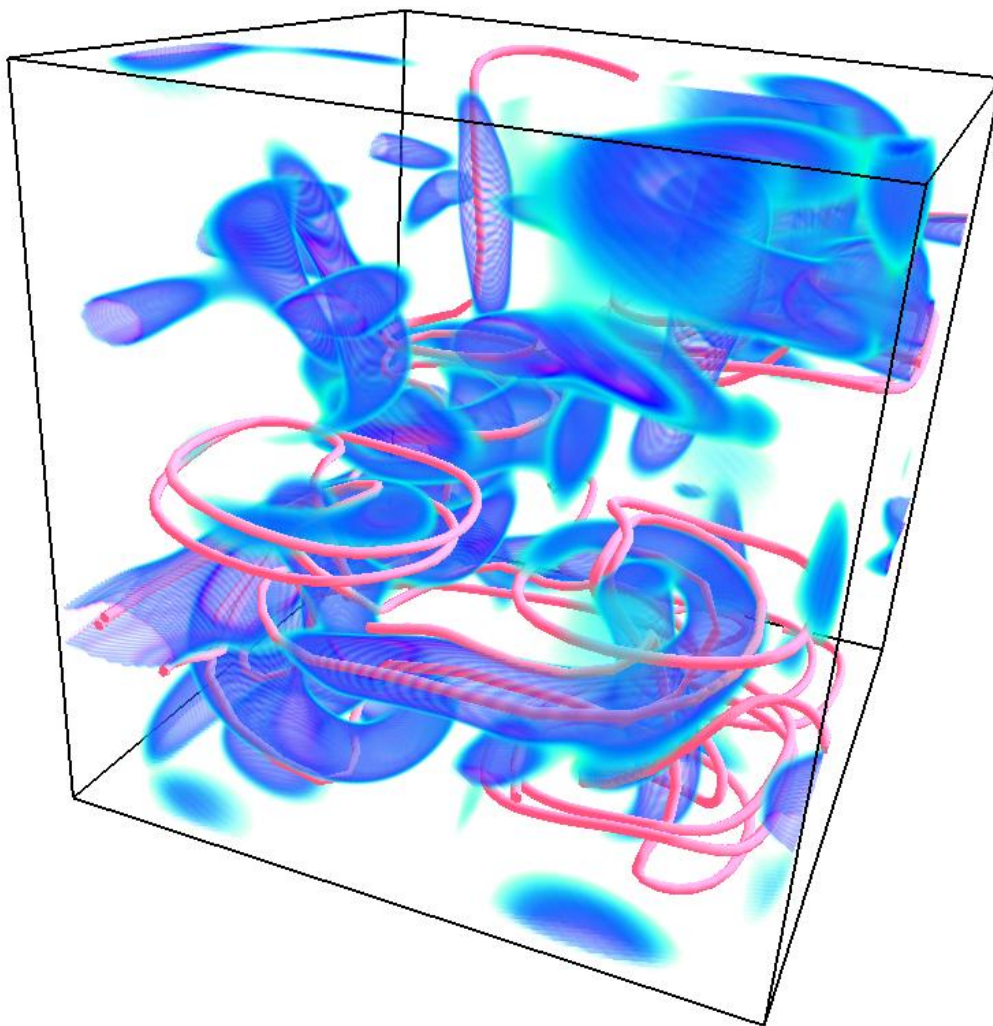


Figure 1: *Volume rendering of the magnetic energy and magnetic field lines from the average in time velocity dynamo mode with a Taylor-Green forcing using VAPOR/NCAR software [6].*

Euler-Lagrangian means in rotating, magnetohydrodynamic flows

Andrew Soward¹ and Paul Roberts²

¹*Department of Mathematical Sciences, University of Exeter, Exeter, EX4 4QE, UK*

²*Department of Mathematics, University of California, Los Angeles, CA 90095, USA*

1. Background

In large Reynolds number turbulence, motion occurs on a wide range of length scales varying from the large size L of the of the system down to the very short length viscous length scale l_ν ($\ll L$). Only on that latter length l_ν is viscous dissipation important. For buoyancy driven MHD systems the problem is complicated by the fact that there are in addition other dissipation lengths such as the thermal and magnetic diffusion length scales l_κ and l_η , which may be of very disparate values depending on the Prandtl numbers l_ν/l_κ and l_ν/l_η . Since the length scale range between L and $l_{\max} \equiv \max(l_\nu, l_\kappa, l_\eta)$ is so large, it remains problematic, how to deal with the short lengths l ($\ll L$), even when they remain large compared to the diffusion lengths $l \gg l_{\max}$. This is exactly the range that has motivates our enquiry and to which we restrict attention.

In rotating MHD systems, it is well known that the Lagrangian (rather than the Eulerian) representation can often be used very effectively, when $l \gg l_{\max}$. The idea is most readily appreciated in the context of the advection without diffusion of a passive scalar quantity such as temperature, for which its material derivative vanishes. Then the temperature remains constant following fluid particles. Likewise in the case of magnetic field in a perfectly conducting fluid, magnetic flux is conserved on material surfaces. Then the magnetic field at a point moving with the fluid is readily derived in the Lagrangian framework simply by properties of the coordinate transformation relating the current position of fluid particles to their original positions.

The properties mentioned are kinematic in nature and ultimately provide a useful description of the advected quantities. To actually determine their temporal evolution, we need to take advantage of the frozen field results when considering the equation of motion. The simplest application of the idea is through the investigation of the stability of a static state. Since the pressure gradient in the equation of motion does not transform nicely from a Lagrangian point of view, it is better to consider the equation of motion in its Eulerian form. The Eulerian values of the perturbation values of frozen quantities like the magnetic field, which appear in the equation of motion, are determined from their Lagrangian description in terms of the small fluid particle displacement. In this way, equations like the temperature and magnetic induction equations are bypassed leaving only equations for the fluid particle displacement. Even when the background state is moving the essence of this procedure may still be used, albeit a hybrid Eulerian–Lagrangian approach must be adopted instead, as explained in §2, and expressions for the perturbation velocity become more complicated (see, e.g., Frieman and Rotenberg [1]). Though we have outlined the linear ideas in terms of stability calculations, the idea is also useful in the description of wave motions.

Once the fluid particle displacements are no longer small, two distinctive situations need to be distinguished. On the one hand, the displacements may increase indefinitely, as is common in turbulence. For such problems involving (say) the transport of a passive scalar, the Lagrangian procedure has been adopted and used to obtain Eulerian values at quadratic order in the displacement. Then averaging may be used to determine the evolution of the Eulerian mean quantity. On the other, when the particle path displacements ξ (introduced in §2 below and employed in [1]) though finite remain of moderate size, as exemplified by wave turbulence, then the hybrid Eulerian–Lagrangian approach of §2, which builds on the early work of Eckart [2], provides a good way of addressing the evolution of the mean fields correct to $\mathcal{O}(|\xi|^2)$. It was developed by Soward [3] in the dynamo context and Andrews and McIntyre [4] in the atmospheric science context.

2. Methodology

We relate the actual position \mathbf{x}^* of a fluid element at time t^* to a reference position \mathbf{x} at time t by a mapping $\mathbf{x}^* = \mathbf{x}^*(\mathbf{x}, t)$, $t^* = t$. It is simply a time dependent co-ordinate transformation which is complicated by the motion $\mathbf{w}^*(\mathbf{x}, t) = \partial\mathbf{x}^*/\partial t$. The underlying idea is to construct the governing equations relative to the reference frame. To that end we transform our field variables such as the flow velocity $\mathbf{v}^*(\mathbf{x}^*, t^*)$ to form, in the language of the General Tensor Calculus, contravariant and covariant vectors \mathbf{v} and \mathbf{V} defined by

$$v_i^* = v_j \partial x_j^* / \partial x_i = V_j \partial x_j / \partial x_i^* \quad \text{together with} \quad w_i^* := \partial x_i^* / \partial t = w_j \partial x_j^* / \partial x_j = W_j \partial x_j / \partial x_i^*.$$

In view of the pressure gradient in the equation of motion, it is convenient to write it in covariant form with momentum proportional to \mathbf{V} , which in turn relates to circulation $\oint \mathbf{v}^* \cdot d\mathbf{x}^* = \oint \mathbf{V} \cdot d\mathbf{x}$. On the other hand, the rate of working of a body force \mathbf{F}^* is $\mathbf{v}^* \cdot \mathbf{F}^* = \mathbf{v} \cdot \mathbf{F}$, where \mathbf{F} is the resulting covariant body force in the transformed equation of motion. The material derivative needed in the advection of momentum (or any other advected quantity for that matter) takes the form

$$D/Dt^* := \partial/\partial t^* + \mathbf{v}^* \cdot \nabla^* = \partial/\partial t + \mathbf{u} \cdot \nabla =: D/Dt,$$

in which $\mathbf{u} = \mathbf{v} - \mathbf{w}$ is the contravariant form of the advective velocity $\mathbf{v}^* - \mathbf{w}^*$ in the moving $\mathbf{x}^*(\mathbf{x}, t)$ -frame.

The three velocities \mathbf{u} , \mathbf{v} and \mathbf{V} , which we have identified, have an important role to play in the hybrid Eulerian–Lagrangian approach. In practise to use them we consider small displacements $\mathbf{x}^* - \mathbf{x}$ and write

$$\mathbf{v}^*(\mathbf{x}^*, t^*) = D\mathbf{x}^*/Dt^* = \mathbf{u} + D\boldsymbol{\xi}/Dt, \quad \text{where} \quad \mathbf{x}^*(\mathbf{x}, t) = \mathbf{x} + \boldsymbol{\xi}(\mathbf{x}, t) \quad (L \gg |\boldsymbol{\xi}| \gg l_{\max}).$$

We take statistical averages $\overline{\quad}$ and demand that $\overline{\mathbf{u}} = \mathbf{u}$ and $\overline{\boldsymbol{\xi}} = \mathbf{0}$. By this device \mathbf{u} is the the Lagrangian average of $\mathbf{v}^*(\mathbf{x}^*, t^*)$ (i.e. at fixed \mathbf{x} following the motion of the fluctuating displacement $\boldsymbol{\xi}$).

3. Results

We outline the equations for the contravariant and covariant vector fields that emerge from the governing equations of the full rotating MHD system (as reviewed in [5]). Holm [6] calls them the Generalised Lagrangian Mean (GLM) equations. We consider their expansions up to $\mathcal{O}(|\boldsymbol{\xi}|^2)$ extending on the earlier developments of [3], [4] and [6]. Holm has also proposed an Eulerian counterpart which he calls the generalised lagrangian mean (glm) equations derived from Hamilton’s principle applied to an averaged Lagrangian. The new equations are motivated by the wish to have an Eulerian formulation which contains the merits of the GLM system (such as the conservation of mean circulation for Euler’s equations). We consider the relation between the GLM and glm systems as formulated in terms of Eulerian variables. The absence of certain $\mathcal{O}(|\boldsymbol{\xi}|^2)$ terms in the glm system suggests that they have been filtered out on averaging the Lagrangian.

References

- [1] E. Frieman and M. Rotenberg 1960 *On hydromagnetic stability of stationary equilibria*, Rev. Mod. Phys., **32**, 898 – 902.
- [2] C. Eckart 1963 *Some transformations of the hydrodynamic equations*, Phys. Fluids, **6**, 1037 – 1041.
- [3] A. M. Soward 1972 *A kinematic theory of large magnetic Reynolds number dynamos* Phil. Trans. R. Soc. Lond. **A272**, 431 – 462
- [4] D. G. Andrews and M. E. McIntyre 1978 *An exact theory of nonlinear waves on a Lagrangian-mean flow*, J. Fluid Mech., **89**, 609 – 646.
- [5] P. H. Roberts and A. M. Soward 2006 *Eulerian and Lagrangian means in rotating, magnetohydrodynamic flows I. General results*, Geophys. Astrophys. Fluid Dynam., **100**, 000 – 000.
- [6] D. D. Holm 2002 *Averaged Lagrangians and mean effects of fluctuations in ideal fluid dynamics*, Physica D, **170**, 253 – 286.

Preliminary results from a new incompressible spectral element MHD solver in the Geophysical-astrophysical spectral-element adaptive mesh (GASpAR) code

Duane Rosenberg, Pablo Mininni, Annick Pouquet, & Aimé Fournier

National Center for Atmospheric Research, P.O. Box 3000, Boulder, CO, 80307-3000, USA

Accurate and efficient simulation of strongly turbulent flows is a prevalent challenge in many atmospheric, oceanic, and astrophysical applications. New simulation codes are being developed to investigate such flows in the parameter regimes that interest the scientific communities corresponding to these application areas.

In the case of nonmagnetized fluids, nonlinearities prevail when the Reynolds number Re is large. The number of degrees of freedom in three dimensions increases as $Re^{9/4}$ as Re tends to infinity in the Kolmogorov 1941 framework. For geophysical and astrophysical flows, often $Re \gg 10^8$. Computations of turbulent flows must contain enough scales to encompass the energy-containing and dissipative scale ranges distinctly. Three-dimensional compressible flow simulations show that in order to achieve the desired scale ranges, uniform grids must contain at least 2048^3 cells [5], a feat which, today, can barely be accomplished. Indeed, a pseudo-spectral Navier-Stokes code on a grid of 4096^3 uniformly spaced points has been run on the Earth Simulator [2], with a Taylor Reynolds number ($\propto \sqrt{Re}$) of ≈ 1200 , still far from what is required for most geophysical and astrophysical flows.

We have been engaged in the development of a high-order code for modeling turbulence in a variety of systems. Our code, the geophysical and astrophysical spectral-element adaptive refinement (GASpAR) code, is an object-oriented framework for solving PDEs using high-order adaptive methods. Like most spectral-element codes, GASpAR combines finite-element efficiency with spectral-method accuracy. It is designed to be flexible enough for a range of geophysics and astrophysics applications where turbulence or other complex multi-scale problems arise. The formalism accommodates both conforming and non-conforming elements, and it includes a new formulation of dynamic adaptive refinement (DARE) of non-conforming h-type [4], with the order of polynomials in each element kept fixed. The code has been tested thoroughly in two space dimensions, but is written in a modular fashion that can be extended readily to three dimensions.

One of the main goals of our development effort is to ask, if the significant structures of the flow are indeed sparse, so that their dynamics can be followed accurately even if they are embedded in random noise, then does dynamic adaptivity offer a means for achieving an otherwise unattainable large (effective) number of degrees of freedom? The figure represents an example of adaptivity for the merger of three vortices for two dimensional Navier-Stokes as also computed in [3].

A new spectral-element solver for incompressible magnetohydrodynamics (MHD) has recently been developed for the GASpAR code based on the Elsässer formulation [1]. This solver, like the existing ones, automatically takes advantage of the DARE capability offered by the code, as well as of other user-defined administration features.

In this talk, we will describe the MHD solver, and present some preliminary results, primarily with regard to validation in the laminar and turbulent regimes. This description will be couched in a brief discussion of the code and of the DARE methodology. Some examples will be given. We will also discuss some of the issues involved in modeling MHD turbulence using spectral-element methods.

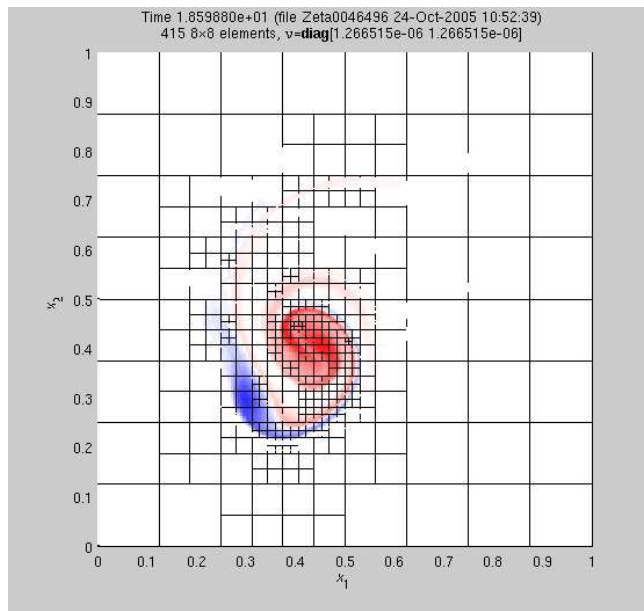


Figure 1: 3-vortex simulation showing merging of two positive (red) and one negative (blue) vortices. Four levels of refinement are used with order 7 in each element.

References

- [1] Elsasser, W.M. 1950. *The hydromagnetic equations*, Phys. Rev. **79**, 183.
- [2] Isihara T., Y. Kaneda, M. Yokokawa, K. Itakura, and A. Uno 2003. *Spectra of energy dissipation, enstrophy and pressure by high-resolution direct numerical simulations of turbulence in a periodic box*, J. Phys. Soc. Japan **72**, 983–986.
- [3] Kevlahan K.-R., and M. Farge 1997. *Vorticity filaments in two dimensional turbulence: creation, stability and effect*, J. Fluid Mech. **346**, 49-76.
- [4] D. Rosenberg, A. Fournier, P. Fischer, and A. Pouquet 2006. *Geophysical-astrophysical spectral-element adaptive refinement (GASpAR): Object-oriented h-adaptive fluid dynamics simulation*, J. Comp. Phys. **215**, 59-80.
- [5] I. Sytine, D. Porter, P. Woodward, S. Hodson and K-H Winkler, 2000. *Convergence tests for the Piecewise Parabolic Method and Navier-Stokes solutions for homogeneous compressible turbulence*, J. Comp. Phys. **158**, 225–238.

Spatially global & local scale-interaction analyses for nonconforming spectral-element simulations

Aimé Fournier

*Institute for Mathematics Applied to Geosciences
National Center for Atmospheric Research, Boulder CO 80307-3000 USA*

The classical mathematical tool to analyze scales in spatial functions $u(\vec{x})$ has been the Fourier basis $F_{\vec{k}}(\vec{x}) := e^{2\pi i \vec{k} \cdot \vec{x}}$. The wavevector \vec{k} labels *global* scale content, i.e., if a certain Fourier component $\hat{u}_{\vec{k}} := \langle F_{\vec{k}}^* u \rangle$ is relatively large then *on average over the spatial domain* the corresponding field $u(\vec{x})$ exhibits relatively significant structure at the corresponding scale $|\vec{k}|^{-1}$. There is information only about scale but not the \vec{x} *location* where the structures occur¹, which can be a serious limitation. Several remedies have been developed to regain that information. Fournier [1, 2, 3], and op. cit. therein, have generalized localized scale interactions (LSI²) from wavevector components $\hat{u}_{\vec{k}}$ to wavelet components $\tilde{u}_{\vec{\ell}} := \langle \psi_{\vec{\ell}}^* u \rangle$ using some basis $\psi_{\vec{\ell}}(\vec{x})$. These LSI analyses offer a multiscale analysis tool for which turbulence science has been striving, for a long time and for many purposes [2, for a review].

Another well known approach to multiscale simulation is adaptive mesh refinement (AMR). All AMR codes involve partitioning the problem's spatial domain \mathbb{D} into disjoint elements $\mathbb{D} = \bigcup_{\vec{\ell} \in \mathbb{L}} \mathbb{X}_{\vec{\ell}}$, and most AMR codes use the finite-element method (FEM) or similar discretizations with a small set of values representing the global solution $u(\vec{x}, t)$ locally in each $\mathbb{X}_{\vec{\ell}}$. Thus *most AMR simulations are intrinsically locally low-order* w.r.t. the $\mathbb{X}_{\vec{\ell}}$ size $h_{\vec{\ell}}$. However, a few AMR codes are locally *high-order* w.r.t. a parameter $p_{\vec{\ell}}$ in each $\mathbb{X}_{\vec{\ell}}$; these include adaptive *spectral-element methods* (SEMs, e.g., [6, 7, 8] and op. cit. therein). The combined **h-p** analyses built into SEM make it very effective for complicated flows [5, 6, 7, 8]. Using SEM combined with LSI, we can quantitatively model and analyze many important phenomena that involve scale interactions localized in parts of the domain, and that heretofore were mainly only described qualitatively or heuristically.

The fundamental cause of scale interactions is the presence of nonlinearities in the governing dynamics. Nonlinear terms such as $\vec{v} \cdot \vec{\nabla} \vec{v}$ at high Reynolds number can generate significant phenomena, such as coherent vortices, fronts, tubes etc. Historically, important and insightful diagnostic tools for understanding these interactions have been linked to “spectral energetics”, e.g., the analysis of Fourier spectra and triad interactions³

$$T_{a,b,c}^F := \hat{u}_{\vec{k}_a}^* \cdot (\hat{u}_{\vec{k}_b} \cdot 2\pi i \vec{k}_c \delta_{\vec{k}_a, \vec{k}_b + \vec{k}_c}) \hat{u}_{\vec{k}_c} \quad (1)$$

between modes a, b and c that describe global scale interactions without \vec{x} -location information. Using the $\psi_{\vec{\ell}}$ basis, scale resolution of u is degraded,⁴ from a sharp wavevector value \vec{k} down to *approximate wavevector elements* $\pm \vec{k} \in \mathbb{K}_{\vec{\ell}} := \text{supp } \hat{\psi}_{\vec{\ell}} \approx \times_{\alpha=1}^d [K_{\alpha}, 2K_{\alpha}]$ (where $K_{\alpha} := 2^{\lfloor \log_2 \ell_{\alpha} \rfloor}$), while location information is augmented, from lack-of-information up to element locations $\vec{X} := \vec{K}^{-1} \cdot (\vec{\ell} - \vec{K})$ (where $\vec{K} := \text{diag } K$). We obtain new energetics diagnostics *describing both scale and location*:

$$T_{a,b,c} := \tilde{u}_{\vec{\ell}_a}^* \cdot (\tilde{u}_{\vec{\ell}_b} \cdot \langle \psi_{\vec{\ell}_a}^* \psi_{\vec{\ell}_b} \vec{\nabla} \psi_{\vec{\ell}_c} \rangle) \tilde{u}_{\vec{\ell}_c}, \quad (2)$$

¹Location information is dispersed among all arg $\hat{u}_{\vec{k}}$.

²Apologies to *the Shamen*.

³In practice, $T_{a,b,c}$ is symmetrized to isolate boundary-flux or divergent- \vec{v} contributions so that “detailed conservation” $T_{a,b,c} + T_{b,c,a} + T_{c,a,b} = 0$ holds.

⁴As required by the Heisenberg uncertainty principle; note that $|\mathbb{K}_{\vec{\ell}}| \gtrsim \prod_{\alpha=1}^d K_{\alpha} = |\mathbb{X}_{\vec{\ell}}|^{-1}$.

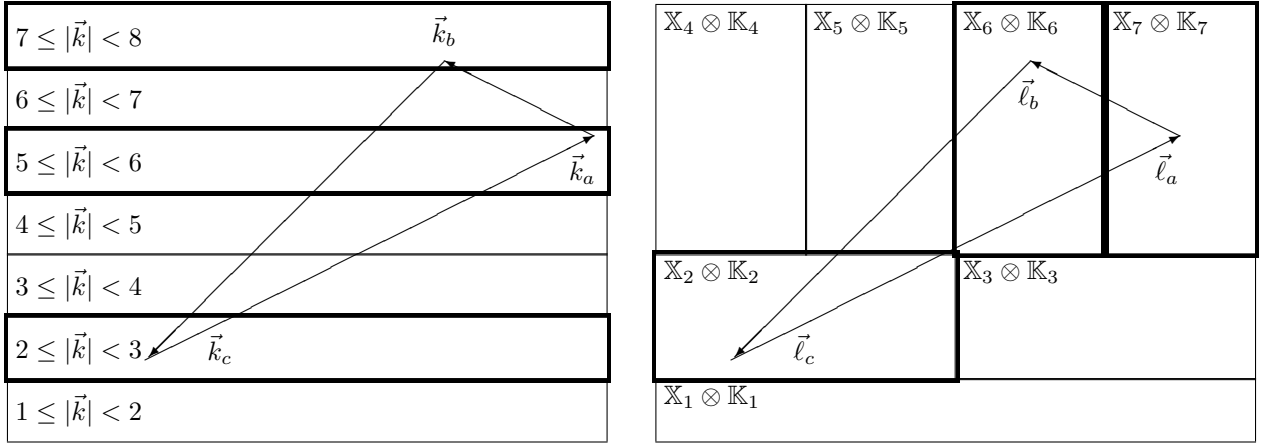


Figure 1: Schematic illustration of triad interaction in Fourier space (1), left, and wavelet space (2), right.

the triadic interaction among three structures in \vec{u} that have characteristic scales \vec{K}_a , \vec{K}_b , \vec{K}_c and locations \vec{X}_a , \vec{X}_b , \vec{X}_c (Fig. 1). One can see that the triad (2) generalizes the Fourier triad (1). In fact, (2) is even more general, in that the $\psi_{\vec{\ell}}$ can be *any* orthogonal basis. In order to construct LSI we may use a SEM basis $\psi_{\vec{\ell}}$ built up from a one-dimensional single-element basis $\psi_j(\xi)$ that can be either Legendre or interpolation polynomials for $0 \leq \xi \leq 1$. In the Legendre case the indexes \vec{j} augment the spectral resolution, while in the interpolation case they augment the spatial resolution.⁵ Recently it was shown that it is also possible to use a SEM basis to compute (1) to machine precision [4].

References

- [1] A. Fournier 1995. *Wavelet zonal spectral analysis of observed geopotential and winds: Scale-orthogonal decomposition of blocking patterns and local kinetic energy and enstrophy transfer between scales*, Eos, Trans. Amer. Geophys. Union **76**, Fall Meet. Suppl. Abstract A41A-02.
- [2] A. Fournier 2003. *Atmospheric energetics in the wavelet domain II: Time-averaged observed atmospheric blocking*, J. Atmos. Sci. **60**, 319–338.
- [3] A. Fournier 2005. *Instantaneous wavelet energetic transfers between atmospheric blocking and local eddies*, J. Climate **13**, 2151–2171.
- [4] A. Fournier 2006. *Exact calculation of Fourier series in nonconforming spectral-element methods*, J. Comp. Phys. **215**, 1–5.
- [5] A. Fournier, G. Beylkin and V. Cheruvu 2005. *Multiresolution adaptive space refinement in geophysical fluid dynamics simulation*, Lecture Notes Comp. Sci. Eng. **41**, 161–170.
- [6] A. Fournier, M.A. Taylor and J.J. Tribbia 2004. *The spectral element atmosphere model (SEAM): High-resolution parallel computation and localized resolution of regional dynamics*, Mon. Wea. Rev. **132**, 726–748.
- [7] D. Rosenberg and A. Fournier 2006. Presented elsewhere in this Workshop.
- [8] D. Rosenberg, A. Fournier, P. Fischer and Annick Pouquet 2006. *Geophysical-astrophysical spectral-element adaptive refinement (GASpAR): Object-oriented h-adaptive fluid dynamics simulation*, J. Comp. Phys. **215**, 59–80.

⁵One must also high-pass filter to remove the large-scale polynomial space $\mathbb{P}_{\vec{\ell}}(\mathbb{X}_{\vec{\ell}})$ from the union $\bigcup_i \mathbb{P}_{\vec{\ell}}(\mathbb{X}_{i,\vec{\ell}})$ of its subdivided spaces, where $\bigcup_i \mathbb{X}_{i,\vec{\ell}} = \mathbb{X}_{\vec{\ell}}$ and $\mathbb{X}_{i,\vec{\ell}} \cap \mathbb{X}_{i' \neq i, \vec{\ell}} = \emptyset$.

Turbulent cascades in MHD

Alexandros Alexakis,¹ Pablo Mininni,¹ and Annick Pouquet¹

¹*National Center for Atmospheric Research, P.O. Box 3000, Boulder, CO, 80307-3000, USA*

GTP Workshop on
Modeling MHD Turbulence; Applications to Planetary and Stellar dynamos
at the National Center for Atmospheric Research(NCAR),
27-30 June, 2006, Boulder, CO, USA .

Ever since the phenomenological description of Hydrodynamic turbulence by Kolmogorov in 1941 there have been many attempts to derive a similar description for turbulence in conducting fluids (i.e Magneto-Hydrodynamic turbulence). However such a description is going to be based inevitably on strong assumptions that do not necessarily carry over from the Hydrodynamic case. In this talk I will discuss some of the properties of the energy and helicity cascade in turbulent MHD [5, 6, 4, 2] flows and focus on the differences with the hydrodynamic case [3, 1]. The investigation is going to be based on the analysis of transfer functions obtained from high resolution direct numerical simulations. Our results show that the transfer of kinetic energy from the large scales to kinetic energy at smaller scales, and the transfer of magnetic energy from the large scales to magnetic energy at smaller scales, are local, as is also found in the case of neutral fluids, and in a way that is compatible with Kolmogorov (1941) theory of turbulence. However, the transfer of energy from the velocity field to the magnetic field is a highly nonlocal process in Fourier space. Energy from the velocity field at large scales can be transferred directly into small scale magnetic fields without the participation of intermediate scales. The cascade of magnetic Helicity in MHD appear to be even more non-local processes. Some implications of these results to turbulent cascade models will be discussed.

References

- [1] P.Mininni, A. Alexakis, A. Pouquet, (2006) *Large scale flow effects, energy transfer, and self-similarity on turbulence* submitted to: Phys. Rev E <http://arxiv.org/pdf/physics/0602148>
- [2] P. Mininni, A. Alexakis, A. Pouquet, (2006) *Energy transfer in Hall-MHD turbulence: cascades, backscatter, and dynamo action*, J. Plasma Physics (2005) <http://arxiv.org/pdf/physics/0510053>
- [3] A. Alexakis, P. Mininni, A. Pouquet, *The imprint of large scale flows on turbulence*, Phys Rev. Let. **95** 264503
- [4] A. Alexakis, P. Mininni, A. Pouquet (2006) *On the inverse cascade of Magnetic Helicity*, Astrophys. J. **640** 335–343
- [5] A. Alexakis, P. Mininni, A. Pouquet (2005) *Shell to shell energy transfer in MHD, Part I: steady state turbulence*, Phys. Rev. E **72** 046301
- [6] P. Mininni, A. Alexakis, A. Pouquet *Shell to shell energy transfer in MHD, Part II: Kinematic dynamo*, Phys. Rev. **72** 046302

Intermittency in MHD turbulence: DNS and Lagrangian averaged modeling

Jonathan Pietarila Graham,¹ Pablo Mininni,¹ Annick Pouquet,¹ and Darryl Holm^{2,3}

¹*National Center for Atmospheric Research, P.O. Box 3000, Boulder, CO, 80307-3000, USA*

²*Department of Mathematics, Imperial College London, London SW7 2AZ, UK*

³*Computer and Computational Science Division, Los Alamos National Laboratory, Los Alamos, NM
87545, USA*

Subgrid modeling of MHD flows is still under development. Most LES for hydrodynamic turbulence are based upon self-similarity or universality, in that they assume a known power law of the energy spectrum. For MHD, the kinetic energy is not a conserved quantity, and this poses a problem for the extension of such techniques to this case. Additional difficulties arise from the fact that MHD has several regimes depending on the relative strengths of the magnetic and velocity fields, their degree of alignment, and whether mechanical or magnetic energy is injected into the flow. However, some LES have been developed for particular cases. There exists LES for MHD turbulence with some degree of alignment between the fields, dissipative LES which does not model the interactions between the two fields, and LES for low magnetic Reynolds number (see [1] for references). A more generally applicable subgrid model that would also handle transitional flows (e.g. dynamos) is then desirable. To this end, we investigate the Lagrangian averaged magneto-hydrodynamic alpha (*LAMHD*– α) model. This model we have recently tested both in 2D and in 3D and it has been used to examine the onset of the dynamo instability when the magnetic Prandtl number is small. Most of these works compared the time evolution of ideal invariants for forced and free decaying turbulence, as well as the evolution of energy spectra. Also, some statistical comparisons were performed (e.g. studying the behavior of probability density functions). In this work, we apply a more stringent test to this model. Intermittency is a well known feature of turbulent flows, associated with the existence of strong events localized both in space and time. Intermittency can trigger large scale events, affect the transport coefficients, or give rise to corrections in the turbulent scaling. As a result, whether a subgrid model can capture the statistics of intermittent events is of utmost importance to model astrophysical or geophysical flows. This study also requires high order statistics, thereby extending comparisons between direct numerical simulations (DNS) and α -models.

The equations for *LAMHD*– α are

$$\begin{aligned} \partial_t \mathbf{u} + \mathbf{u}_s \cdot \nabla \mathbf{u} - \mathbf{B}_s \cdot \nabla \mathbf{B} + (\nabla \mathbf{u}_s)^T \cdot \mathbf{u} + (\nabla \mathbf{B})^T \cdot \mathbf{B}_s + \nabla \pi = \nu \Delta \mathbf{u}, \\ \partial_t \mathbf{B}_s + \mathbf{u}_s \cdot \nabla \mathbf{B}_s - \mathbf{B}_s \cdot \nabla \mathbf{u}_s = \eta \Delta \mathbf{B}, \end{aligned} \quad (1)$$

where \mathbf{u} and \mathbf{B} are the velocity and magnetic fields (both divergence free), ν is the viscosity, and η is the diffusivity. The subscript s denotes smoothing obtained by inverting the relations, $\mathbf{u} = (1 - \alpha^2 \Delta) \mathbf{u}_s$, $\mathbf{B} = (1 - \alpha_M^2 \Delta) \mathbf{B}_s$. We compare intermittency in (1) to that of DNS of MHD, regarded as true at a given Reynolds number. We define the longitudinal structure function of the Elsässer variable $\mathbf{z}^+ = \mathbf{u} + \mathbf{B}$ as $S_p^+(l) \equiv \langle |\delta z_L^+|^p \rangle$ where $\delta z_L^+ = (\mathbf{z}^+(\mathbf{x} + \mathbf{l}) - \mathbf{z}^+(\mathbf{x})) \cdot \mathbf{l} / l$ is the longitudinal increment of \mathbf{z}^+ . Four sets of 2D simulations were computed with periodic boundary conditions, one set of MHD DNS with 1024^2 grid points, and three sets of *LAMHD*– α simulations, 512^2 and $\alpha = \alpha_M = 6/512$, 256^2 and $\alpha = \alpha_M = 6/256$, and 256^2 and $\alpha = \alpha_M = 6/128$. All simulations were identical with regards to dissipation ($\eta = \nu = 1.6 \times 10^{-4}$) and forcing (in the Fourier ring $k = [1, 2]$ with random phases in momentum and vector potential).

With the Extended Self-Similarity (ESS) hypothesis we determined the relative scaling exponents, ξ_p^+ , from $S_p^+(l) \sim [L^+(l)]^{\xi_p^+}$ where $L^+ \propto l$ from the Kármán-Howarth theorem (see [1] for details). Figure 1

compares the scaling exponent, ξ_p^+ , for the DNS runs and the three sets of *LAMHD*– α runs. In the figure, the She-Lévêque (SL) formula for MHD is shown as a reference, $\frac{\xi_p^+}{\xi_3^+} = \frac{p}{6} + 1 - \left(\frac{1}{2}\right)^{p/3}$. The α –model captured the high-order statistics and the anomalous scaling of the longitudinal structure function exponents (to within the errors of our statistics), with a net gain in speed close to a factor of 16. For lower order structure functions, very little contamination of the scaling could be detected at scales larger than α .

In current sheets, where magnetic reconnection occurs, the magnetic field and the current rapidly change sign. To preserve reliable statistics of these events in subgrid models of MHD turbulence is of importance in many problems. In order to measure fast oscillations in sign of a field on arbitrary small scales, the cancellation exponent was introduced (see [2] for references). The signed measure for the current $j_z(\mathbf{x})$ on a set $Q(L)$ of size L is $\mu_i(l) = \int_{Q_i(l)} d\mathbf{x} j_z(\mathbf{x}) / \int_{Q(L)} d\mathbf{x} |j_z(\mathbf{x})|$ where $\{Q_i(l)\} \subset Q(L)$ is a hierarchy of disjoint subsets of size l covering $Q(L)$. The partition function χ measures the cancellations at a given lengthscale l , $\chi(l) = \sum_{Q_i(l)} |\mu_i(l)|$. We can study the scaling behaviors of the cancellations defining the cancellation exponent κ , where $\chi(l) \sim l^{-\kappa}$. Positive κ indicates fast changes in sign on small scales. This exponent can also be related with the fractal dimension D of the structures, $\kappa = (d - D)/2$, where d is the number of spatial dimensions of the system. The evolution of the cancellation exponent as a function of time for free decaying simulations is shown in Fig. 2. The maximum of κ takes place slightly later than the maximum of magnetic dissipation. Note that the alpha-model captures the time evolution of the cancellation exponent, as well as the fractal structure of the problem as time evolves.

Future challenges will include implementation of *LAMHD*– α in domains with boundaries and the study of intermittency for magnetic Prandtl numbers besides unity.

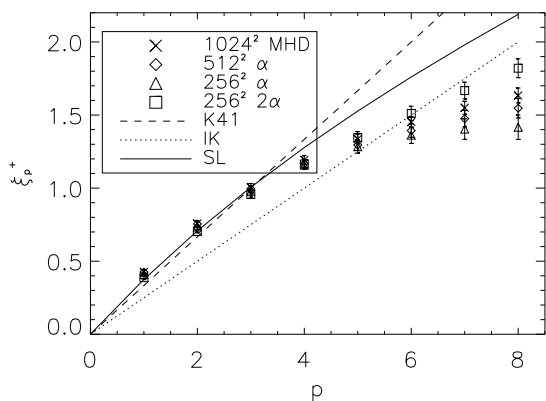


Figure 1: Structure function scaling exponent: ξ_p^+ versus p . 1024^2 MHD are the pluses, for *LAMHD*– α 512^2 are the diamonds, 256^2 ($\alpha = 6/256$) are triangles, and 256^2 ($\alpha = 6/128$) are the squares. The error bars are the error to the least-squares fit.

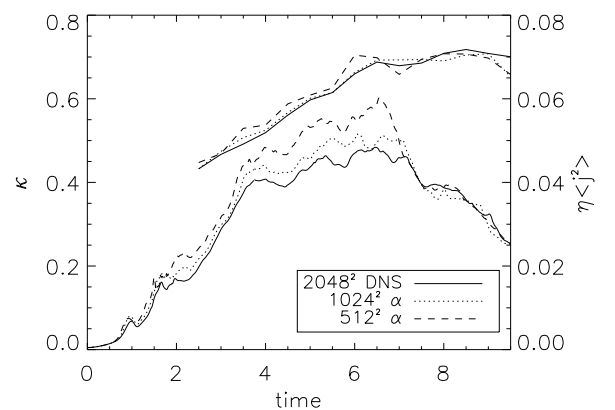


Figure 2: Time history of the cancellation exponent (thick lines) for the three free decaying runs, and of $\eta \langle j_z^2 \rangle$, where the brackets denote spatial average.

References

- [1] J. Pietarila Graham, D. D. Holm, P. Mininni, and A. Pouquet 2006. *Inertial range scaling, Kármán-Howarth theorem, and intermittency for forced and decaying LAMHD– α in 2D*, Phys. Fluids **18**, 045106.
- [2] J. Pietarila Graham, P. D. Mininni, and A. Pouquet 2005. *Cancellation exponent and multifractal structure in 2D MHD: Direct numerical simulations and LAMHD– α* , Phys. Rev. E **72**, 045301.

Scale-similar models for large eddy simulations of a rotating convection-driven dynamo

Qiaoning Chen

Institute of Geophysics and Planetary Physics, University of California, Los Angeles, CA 90095

The scale-similar model of [1] *et al.* and a dynamic similarity model have been applied to a rotating convection-driven dynamo simulation. The results from the similarity model, using unit constant coefficients, are satisfactory: the large-scale magnetic/kinetic energies and *r.m.s* magnetic/velocity field fluctuations are in much better agreement with the highly-resolved solution than with the low resolution simulation. The model is found to be much less sensitive to the filter scale than the *a priori* test. Implementation of a dynamic procedure to the similarity model gives better agreement provided that the two filtering scales are properly chosen. The model coefficients from the dynamic procedure are less than 1.0, in the range [0.4, 0.8].

[A mathematical dynamo model]

Equations: The governing Boussinesq equations for a rotating convection-driven plane layer dynamo

$$\mathbf{e}_z \times \mathbf{v} = -\nabla p + (\nabla \times \mathbf{B}) \times \mathbf{B} + qRa\mathbf{e}_z T + Ek\nabla^2 \mathbf{v}, \quad (1)$$

$$\frac{\partial \mathbf{B}}{\partial t} = \nabla \times (\mathbf{v} \times \mathbf{B}) + \nabla^2 \mathbf{B}, \quad (2)$$

$$\frac{\partial T}{\partial t} + \mathbf{v} \cdot \nabla T = q\nabla^2 T + v_z, \quad (3)$$

$$\nabla \cdot \mathbf{v} = 0, \quad \nabla \cdot \mathbf{B} = 0. \quad (4)$$

Here \mathbf{v} , \mathbf{B} and T are the dimensionless velocity, magnetic field and temperature fluctuation, respectively. The dimensionless t is the magnetic diffusion time. The Roberts number $q = \kappa/\eta$, the modified Rayleigh number $Ra = g\bar{\alpha}\bar{\beta}d^2/2\Omega\kappa$, the Ekman number $Ek = \nu/2\Omega d^2$ and the magnetic Ekman number $Ek_\eta = \eta/2\Omega d^2$.

[Large-eddy simulation]

In the LES approach, the large-scale velocity $\bar{\mathbf{v}}$ is obtained by convolution, through a spatial filter function $G_\Delta(r, x)$ [2]:

$$\bar{\mathbf{v}}(\mathbf{x}, t) = \int G_\Delta(\mathbf{r}, \mathbf{x}) \mathbf{v}(\mathbf{x} - \mathbf{r}, t) d\mathbf{r}. \quad (5)$$

where Δ is the filter width. The velocity $\mathbf{v}(\mathbf{x}, t)$ is decomposed into a large-scale (or resolved) part $\bar{\mathbf{v}}$ and a subgrid (or under-resolved) part \mathbf{v}' as $\mathbf{v} = \bar{\mathbf{v}} + \mathbf{v}'$.

Equations: A LES representation of the dynamo model:

$$\mathbf{e}_z \times \bar{\mathbf{v}} = -\nabla \bar{p} + \nabla \times \bar{\mathbf{B}} \times \bar{\mathbf{B}} - \nabla \cdot \boldsymbol{\tau} + qRa\bar{T}\mathbf{e}_z + Ek\nabla^2 \bar{\mathbf{v}}, \quad (6)$$

$$\frac{\partial \bar{\mathbf{B}}}{\partial t} + \bar{\mathbf{v}} \cdot \nabla \bar{\mathbf{B}} = \bar{\mathbf{B}} \cdot \nabla \bar{\mathbf{v}} - \nabla \cdot \boldsymbol{\tau}^B + \nabla^2 \bar{\mathbf{B}}, \quad (7)$$

$$\frac{\partial \bar{T}}{\partial t} + \bar{\mathbf{v}} \cdot \nabla \bar{T} = -\nabla \cdot \mathbf{Q} + \bar{v}_z + q \nabla^2 \bar{T}, \quad (8)$$

$$\nabla \cdot \bar{\mathbf{v}} = 0, \quad \nabla \cdot \bar{\mathbf{B}} = 0. \quad (9)$$

[The subgrid-scale(SGS) terms]

The influence of the subgrid-scales on the resolved scales is embedded in SGS terms:

1. *Reynolds stress:*

$$\boldsymbol{\tau} = Ek_\eta (\overline{\mathbf{v}\mathbf{v}} - \bar{\mathbf{v}}\bar{\mathbf{v}}) - (\overline{\mathbf{B}\mathbf{B}} - \bar{\mathbf{B}}\bar{\mathbf{B}}), \quad (10)$$

2. *Turbulent electromotive force (emf):*

$$\boldsymbol{\tau}^B = \overline{\mathbf{v}\mathbf{B}} - \bar{\mathbf{v}}\bar{\mathbf{B}} - (\overline{\mathbf{B}\mathbf{v}} - \bar{\mathbf{B}}\bar{\mathbf{v}}), \quad (11)$$

3. *Heat flux:*

$$\mathbf{Q} = \overline{\mathbf{v}T} - \bar{\mathbf{v}}\bar{T}. \quad (12)$$

In our investigation the inertial forces are negligible, the magnetic Ekman number $Ek_\eta = 2\Omega/\eta$ is zero, so the Reynolds stress $\boldsymbol{\tau}$ reduces to $\boldsymbol{\tau} = -\boldsymbol{\tau}^{Max}$ where $\boldsymbol{\tau}^{Max} = \overline{\mathbf{B}\mathbf{B}} - \bar{\mathbf{B}}\bar{\mathbf{B}}$ is generally called ‘the Maxwell stress tensor’.

[The similarity model]

We model the SGS terms using the similarity model.

1. *Maxwell stress:*

$$\boldsymbol{\tau}_{sim}^{Max} = C_{mom} (\widetilde{\overline{\mathbf{B}\mathbf{B}}} - \widetilde{\bar{\mathbf{B}}}\widetilde{\bar{\mathbf{B}}}), \quad (13)$$

2. *Turbulent electromotive force:*

$$\boldsymbol{\tau}_{sim}^B = C_{ind} (\widetilde{\overline{\mathbf{v}\mathbf{B}}} - \widetilde{\bar{\mathbf{v}}}\widetilde{\bar{\mathbf{B}}} - (\widetilde{\overline{\mathbf{B}\mathbf{v}}} - \widetilde{\bar{\mathbf{B}}}\widetilde{\bar{\mathbf{v}}}), \quad (14)$$

3. *Heat flux:*

$$\mathbf{Q}_{sim} = C_T (\widetilde{\overline{\mathbf{v}T}} - \widetilde{\bar{\mathbf{v}}}\widetilde{\bar{T}}). \quad (15)$$

where, $\widetilde{}$ represents a second filtering operation at a scale λ with $\lambda/\Delta \geq 1$. The model coefficients $C_{mom} = C_{ind} = C_T = 1$ in the similarity model. In a dynamic similarity model, these models can be adjusted to vary in time and space, i.e. $C_{mom}(z, t), C_{ind}(z, t), C_T(z, t)$.

References

- [1] J. Bardina, J.H. Ferziger and W.C. Reynolds 1980. *Improved subgrid scale models for large-eddy simulations*, Am. Inst. Aeronaut. Astronaut. J., **34**, 1111–1119.
- [2] A. Leonard 1974. *Energy cascade in large-eddy simulations of turbulent flow*, Adv. Geophys., **18**, 237–248.

Dynamic Sub-Grid Scale Modelling of Drift Wave Turbulence within Magnetohydrodynamics

C.J. McDevitt and P.H. Diamond

Center for Astrophysics and Space Sciences and Department of Physics, University of California at San Diego, La Jolla, CA 92093-0424, USA

Modelling disparate scale interactions within MHD remains an ongoing theoretical and computational challenge. In order to facilitate computation, high Reynolds number systems are often described via the introduction of phenomenological dissipation coefficients as a means of modelling stresses exerted by the unresolved scales. The temporal and spatial evolution of these phenomenological coefficients are usually described via heuristic turbulence models. As the dynamics of the unresolved scales play a crucial role in the evolution of the overall system, especially in cases where inverse cascades are present, a simple dynamic sub-grid scale model for the unresolved turbulent scales, that is rigorously derivable from the original fluid equations, is clearly desirable.

In this work, we present a minimal self-consistent model of the multi-scale interaction of large scale MHD flows with small scale drift wave turbulence. Here we utilize the temporal and spatial scale separation between the large scale MHD flows and the small scale drift wave turbulence to separate the system into a set of resolved and unresolved variables. Wave kinetics and adiabatic theory are used to treat the feedback of the large scale MHD flows on the drift waves via shearing and advection. The stresses exerted by the self-consistently evolved drift wave population density on the MHD flows are calculated by mean field methods. This model has the advantage of being both systematically derivable from the original fluid equations without introducing any free parameters, as well as being simple to implement. The principal effect of the drift waves is to pump the resonant low- m mode via a negative viscosity, consistent with the classical notion of an inverse cascade in quasi-2D turbulence. This mechanism is similar to that by which drift wave turbulence drives zonal flows [1].

We study, two types of low- m , resonant structures. The first is a localized, electrostatic vortex mode, driven unstable by Reynolds stresses exerted by the unresolved scales. The width of the mode is set by resistively dissipated magnetic field line bending, and whose growth rate is given by $\gamma = \left(|\nu_T|^{2/3} / \eta^{1/3} \right) (v_A q_y / L_s)^{2/3}$, where ν_T is the turbulent viscosity. A unique feature of this mode, is that the inverse cascade is ultimately terminated via Ohmic heating as opposed to collisional damping as is the case of $m=0$ zonal flows.

The second mode is similar to the usual tearing mode as discussed by Furth, Killeen, and Rosenbluth [2], which matches the visco-resistive layer to an MHD exterior via Δ' . The calculation is complicated by the presence of a strong Reynolds stress term emanating from the background turbulence, which induces strong shear flows within the interior layer. In fact, we find that the magnitude of the turbulent stresses exerted by the drift waves are consistent with a gyro-Bohm diffusivity, and thus, usually exceed the magnitude of the inertia term within the tearing mode equations. Outgoing wave boundary conditions are imposed in order to effect the match with the exterior region. The growth rate in the turbulent viscosity dominated regime is given by $\gamma = \left(\eta^{5/6} / |\nu_T|^{1/6} \right) (q_y v_A / L_s)^{1/3} \Delta'$.

References

- [1] P.H. Diamond, S.-I. Itoh, K. Itoh and T.S. Hahm 2005. *Zonal flows in plasma—a review*, Plasma Phys. Control. Fusion **47**, R35 – R161.
- [2] H.P. Furth, J. Killeen and M.N. Rosenbluth 1963. *Finite-Resistivity Instabilities of a Sheet Pinch*, Phys. Fluids **6**, 459 – 484.

Relation between time spectrum of geomagnetic dipole moment and turbulent state in the Earth's core

Ataru Sakuraba,¹ and Yozo Hamano¹

¹*University of Tokyo, Hongo 7-3-1, Tokyo 113-0033, JAPAN*

The Earth's magnetic field is generated by fluid motion in the liquid outer core, where highly turbulent flow is expected because of extremely low viscosity. Since the core is located deep inside the Earth and surrounded by weakly conductive and partially magnetized mantle and crust, it is inherently difficult to infer small-scale features of the core turbulence by direct observation. On the other hand, the geomagnetic dipole moment, which is nearly axial and intrinsically stronger than other multipoles, is a relatively robust index of the geomagnetic field and can be estimated by paleomagnetic observation throughout a long time range, giving the possibility that the turbulent nature is imprinted in its time series.

Consolini *et al.* [1] reported that the geomagnetic power spectral density was found to be proportional to $f^{-11/3}$ by using recent annual mean data at geomagnetic observatories, where f denotes frequency. They concluded that it should be related to turbulent motion at the surface of the core where a strong magnetic field is present. A spectrum of longer time scales can be estimated by historical, archeomagnetic and paleomagnetic data [2]. Recent estimation by Constable and Johnson [3] clearly shows that the power spectral density of the geomagnetic dipole moment has two corner frequencies, the first one being about 0.02 kyr^{-1} (50 kyr in period) that divides frequency ranges proportional to f^0 and $f^{-5/3}$, and the second one being about 2 kyr^{-1} (500 yr in period) from which a higher frequency range follows with a steeper spectral slope. The higher spectral range seems to connect to the one reported by Consolini *et al.* [1]. Although Constable and Johnson did not mention any implications of turbulence, their data seem to tell us much about magnetohydrodynamic motion hidden inside the Earth.

A rate of change of the axial magnetic dipole moment (m_z) can be expressed as the surface integral of the azimuthal electric current density (J_ϕ); that is,

$$\frac{dm_z}{dt} = -\frac{3}{2}\eta c^2 \oint_{r=c} J_\phi \sin^2 \theta d\theta d\phi \equiv S(t), \quad (1)$$

provided that the Earth's core is spherical and surrounded by a solid insulator [4]. Here, (r, θ, ϕ) are the spherical polar coordinates and η and c are the magnetic diffusivity and the radius of the core, respectively. Once the power spectral density $|\tilde{m}_z(f)|^2$ is observed, it is possible to infer that of the surface current integral

$$|\tilde{S}(f)|^2 = (2\pi f)^2 |\tilde{m}_z(f)|^2, \quad (2)$$

implying that $|\tilde{S}|^2$ of the Earth's core would be characterized by three frequency ranges whose slopes are, from lower to higher frequencies, f^2 , $f^{1/3}$ and $f^{-5/3}$, respectively. It is of particular interest that $|\tilde{S}|^2$ has a peak around $f = 2 \text{ kyr}^{-1}$ and a well-known Kolmogorov slope appears in the higher frequency range.

For further investigation, we carried out a computer simulation of three-dimensional, time-dependent, thermally driven spherical MHD dynamo. The model is almost the same as our previous geodynamo model [5], but the Ekman number is slightly lowered to 10^{-5} and artificial hyper-diffusivities are absent. The Prandtl numbers are all unity. The generated magnetic field is dominated by a quasi-stable axial dipole field. The relation (2) is confirmed by calculating \tilde{S} and \tilde{m}_z independently. The calculated power spectral density $|\tilde{S}|^2$ bears a remarkable resemblance to the observed one. Figure 1 shows that $|\tilde{S}|^2$ has a broad peak around the period of 5 kyr that divides the frequency ranges proportional to $f^{1/3}$ and $f^{-5/3}$.

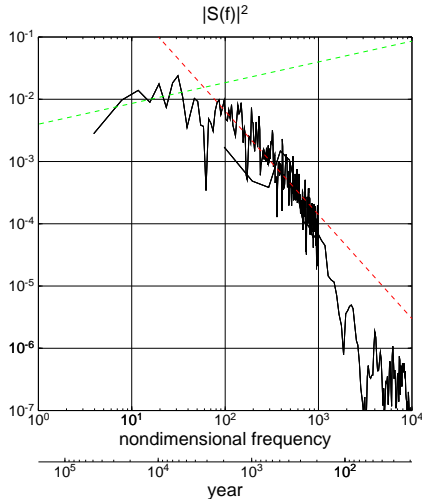


Figure 1: A power spectral density of the surface current integral $|\tilde{S}(f)|^2$ estimated from the numerical model. Two data sets are used to connect lower and higher frequencies. Dotted lines represent $f^{1/3}$ and $f^{-5/3}$ slopes. Time is scaled by $c^2/\eta = 192$ kyr.

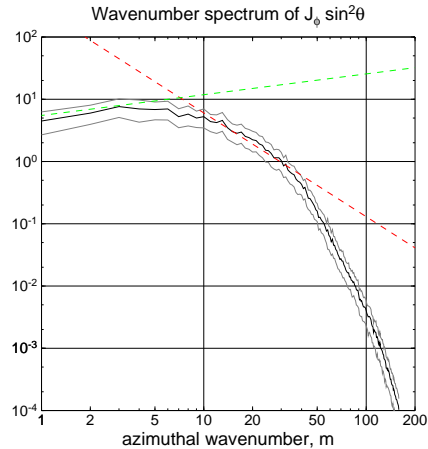


Figure 2: Time-averaged squared Fourier coefficients of $\int J_\phi \sin^2 \theta d\theta$ as a function of the azimuthal wavenumber m . Dotted lines represent $m^{1/3}$ and $m^{-5/3}$ slopes.

The spatial pattern of the surface zonal current looks like a number of small-scale patches of either positive and negative signs. The shape of the patches is so elongated in the θ -direction that the sectorial components dominate when expanded by spherical harmonics. Considering a stochastic behavior of the patches in time and space, we could relate $\tilde{S}(f)$ to the time-averaged wavenumber spectrum of $J_\phi \sin \theta$. Figure 2 indeed shows similarity between them.

The surface electric current reflects the fluid motion inside the core, because an Ekman-Hartmann boundary layer forms beneath the core surface in which Coriolis and Lorentz forces are mutually related. Therefore, $|\tilde{S}|^2$ gives some information about turbulent spectrum of the core. In conclusion, it is suggested that the geomagnetic time spectrum reflects time-averaged small-scale structures of electric current and velocity inside the core. The difference of the peak frequencies in $|\tilde{S}|^2$ spectra between the Earth and the numerical model indicates that the time-averaged electric current and velocity fields in the Earth have typical wavenumber around $m = 50 \sim 100$ and their power decreases in proportion to $m^{-5/3}$ in higher wavenumbers.

References

- [1] G. Consolini, P. Michelis and A. Meloni 2002. *Fluid motions in the Earth's core inferred from time spectral features of the geomagnetic field*, Phys. Rev. E **65**, 037303.
- [2] R. T. Merrill, M. W. McElhinny and P. L. McFadden 1996. *The magnetic field of the Earth* (Academic Press).
- [3] C. Constable and C. Johnson 2005. *A paleomagnetic power spectrum*, Phys. Earth Planet. Inter. **153**, 61–73.
- [4] P. A. Davidson 2001. *An introduction to magnetohydrodynamics* (Cambridge Univ. Press).
- [5] A. Sakuraba and M. Kono 1999. *Effect of the inner core on the numerical solution of the magnetohydrodynamic dynamo*, Phys. Earth Planet. Inter. **111**, 105–121.

A High Order WENO Finite Difference Scheme for Incompressible Fluids and Magnetohydrodynamics

Cheng-Chin Wu

*Institute of Geophysics and Planetary Physics
University of California, Los Angeles, CA 90095*

We present a high-order accurate weighted-essentially-non-oscillatory (WENO) finite difference scheme for solving the motion of incompressible fluids, both for non-magnetic and magnetohydrodynamic (MHD) systems. WENO schemes were originally developed for the compressible Euler equations. They are based on essentially non-oscillatory (ENO) schemes. The key idea in ENO schemes is to approximate the fluxes at the cell boundaries with high order accuracy by using the smoothest stencil among several candidates, and at the same time to avoid spurious oscillations near shocks and discontinuities. The WENO schemes go one step further by taking a weighted average of all candidates. The weights are adjusted by the local smoothness of the solution so that essentially zero weights are given to non-smooth stencils while optimal weights are prescribed in smooth regions. Near discontinuities, WENO schemes and ENO schemes behave in much the same way but, in the smooth regions of the solution, WENO schemes act more like an upstream centered scheme. In principle, any r -th order accurate ENO scheme can be converted into a $(2r-1)$ -th order accurate WENO scheme.

WENO schemes were first developed in a finite volume formulation by Liu, Osher and Chan [1994] for one-dimensional conservation laws. A finite difference version for multidimensional conservation laws was created by Jiang and Shu [1996]. The finite difference WENO scheme was applied to compressible MHD by Jiang and Wu [1999]. Their code forms the basis of this incompressible code.

As in many modern shock capturing methods, WENO schemes are based on local characteristic decomposition of waves and on upwind methods. These two features are equally important for incompressible systems. The wave decomposition of this incompressible MHD code is accomplished by using the characteristic, Elsasser variables. In the code, the WENO method is used in the spatial discretization. High-order Runge-Kutta methods are employed for time integration and the fractional-step method of Kim and Moin [1985] is used to enforce the incompressibility condition.

Numerical results from our new 5th-order accurate code demonstrate that the scheme perform well for one-dimensional Riemann problems, a two-dimensional double-shear flow problem, and the two-dimensional Orszag-Tang MHD vortex system. They establish that the WENO code is numerical stable even when there are no explicit dissipation terms. The code competes on equal terms with pseudo-spectral and spectral methods in regions where the solution is smooth. It can also treat discontinuous data; the method has an advantage over spectral methods in regions where gradients are large.

References

- [1] G.-S. Jiang and C.-W. Shu 1996. *Efficient implementation of weighted ENO schemes*, J. Comput. Phys. **126**, 202 – 228.
- [2] G.-S. Jiang and C.-C. Wu 1999. *A high-order WENO finite difference scheme for the equations of ideal magnetohydrodynamics*, J. Comput. Phys. **150**, 561 – 594.
- [3] J. Kim and P. Moin 1985. *Application of a fractional-step method to incompressible Navier-Stokes equations*, J. Comput. Phys. **59**, 308 – 323.

- [4] X-D. Liu, S. Osher and T. Chan 1994. *Weighted essentially non-oscillatory schemes*, J. Comput. Phys. **115**, 200 – 212.

Intermittent magnetic field excitation by a turbulent flow of liquid sodium

Mark D. Nornberg, Erik J. Spence, Roch D. Kendrick, Craig M. Jacobson,
 and Cary B. Forest

*Department of Physics, University of Wisconsin-Madison
 1150 University Ave., Madison, WI 53706*

Paper submitted to *Phys. Rev. Lett.*

Determining the onset conditions for magnetic field growth in magnetohydrodynamics is fundamental to understanding how astrophysical dynamos such as the Earth, the Sun, and the galaxy self-generate magnetic fields. These onset conditions are now being studied in laboratory experiments using flows of liquid metals [1]. The Madison Dynamo Experiment, currently the largest of the devices, is used to study a flow composed of two counter-rotating helical vortices predicted to produce a growing magnetic field for sufficiently fast flow speeds [2]. The flow is generated by impellers in a 1 m diameter sphere filled with liquid sodium. Liquid metals generally have a low rate of viscous diffusion compared with the rate of resistive diffusion, *e.g.* the Prandtl number for liquid sodium is $Pr = \mu_0 \sigma \nu \sim 10^{-5}$ where σ is the conductivity and ν is the viscosity. Due to the low viscosity, the flows generated in the experiment tend to be quite turbulent. One of the goals of the experiment is to address the effect of turbulence on the threshold conditions for a dynamo.

The threshold of magnetic field generation due to the dynamo instability is governed by the magnetic Reynolds number $Rm = \mu_0 \sigma a v_0$ where a is the radius of the sphere and v_0 is a characteristic flow speed [3]. The magnetic Reynolds number increases for larger impeller rotation rates, and hence larger mean flow speeds. The flow is predicted to generate a magnetic field for $Rm > Rm_{crit}$, where Rm_{crit} is calculated from a model of the mean velocity field constructed from velocity measurements in a full scale water model of the sodium experiment [4]. The structure of the magnetic field generated by the flow is predicted to be a dipolar with an orientation perpendicular to the symmetry axis of the flow as seen in Fig. 1. The growth rate of the field as a function of Rm , shown by the solid curve in Fig. 2, becomes positive for $Rm \geq 190$.

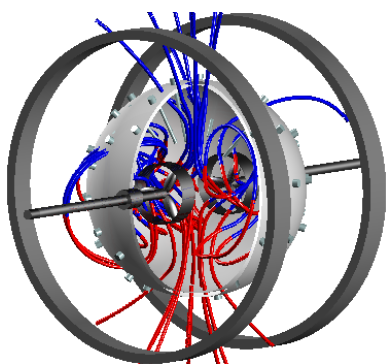


Figure 1: A schematic of the Madison Dynamo Experiment with superimposed magnetic field lines of the theoretically predicted dominant magnetic field.

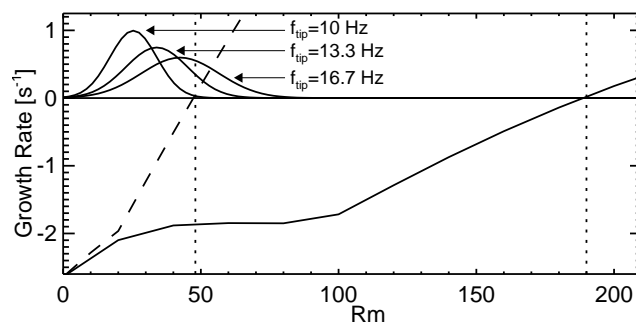


Figure 2: Growth rate of the transverse dipole field versus Rm for the mean flow (solid) and for a slightly different flow geometry (dashed). The vertical lines identify Rm_{crit} for each case. The PDFs of Rm for flows with three different impeller rotation rates are shown to demonstrate the increasing overlap of the ranges of Rm and Rm_{crit} .

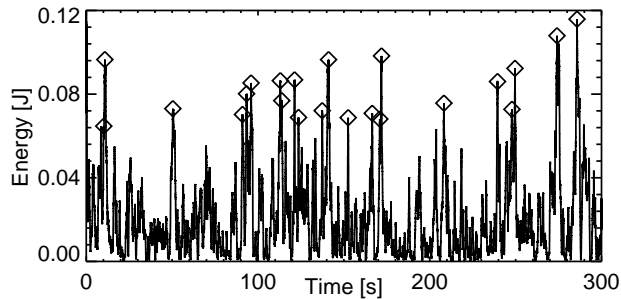


Figure 3: Time series of the energy in the transverse dipole field for an impeller rotation rate of 10 Hz. The diamonds mark the peak of a burst where the energy exceeds 50% of its maximum value.

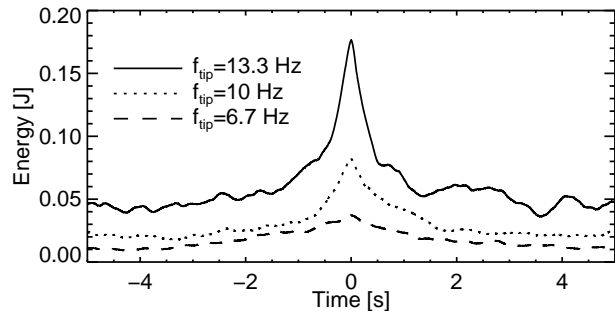


Figure 4: The ensemble average of bursts from three time series. The averaged burst is used to calculate the growth rate.

The mean flow, however, is not the most efficient flow geometry for exciting a magnetic field. A flow with a slightly different geometry has a much lower Rm_{crit} as seen from the dashed curve in Fig. 2 demonstrating that the threshold for field generation is extremely sensitive to the flow geometry.

Due to the simply-connected geometry of the experiment, turbulent eddies range from the viscous dissipation scale (on the order of 1 mm) up to the largest scale of the flow. The large-scale eddies can change the peak flow speed effectively varying Rm . An estimate of the variation in Rm based on the measured velocity fluctuations is shown in Fig. 2. The eddies can also change the flow geometry which can cause significant variations of Rm_{crit} . Thus, although the the mean flow may be subcritical, there can be times for which the instantaneous flow satisfies $Rm > Rm_{\text{crit}}$. The magnetic field momentarily grows while this condition is satisfied and then decays. Hence, the magnetic field is expected to have intermittent bursts.

These bursts are observed in the sodium experiment. Figure 3 shows a time series of the energy in the transverse dipole component of the measured magnetic field. The bursts are ensemble averaged to determine typical characteristics. A burst is defined to occur when the energy in the transverse dipole field exceeds a certain threshold. For this analysis, the threshold is 50% of the maximum energy of the time series. This threshold is sufficiently small to capture a large number of bursts yet significantly larger than the mean energy (about two standard deviations above the mean energy for each time series). The bursts are averaged together and the growth rate is determined by an exponential fit to the curves shown in Fig. 4. The bursts become more frequent and have faster growth rates at larger values of Rm . They become stronger in amplitude but shorter in duration as the turnover time of the large eddies decreases.

The results presented in this paper demonstrate how turbulence in a simply-connected geometry changes the onset conditions of the dynamo. Rather than a smooth transition from damped to growing fields, the transition is characterized by intermittent magnetic field bursts which may be relevant to some dynamo models [5].

References

- [1] A. Gailitis, O. Lielausis, E. Platacis, G. Gerbeth, and F. Stefani, *Rev. Mod. Phys.* **74**, 973 (2002).
- [2] M. L. Dudley and R. W. James, *Proc. R. Soc. London, Ser. A* **425**, 407 (1989).
- [3] H. K. Moffatt, (Cambridge University Press, Cambridge, England, 1978).
- [4] M. D. Nornberg, E. J. Spence, R. D. Kendrick, C. M. Jacobson, and C. B. Forest, *Phys. Plasmas* **13**, 055901 (2006).
- [5] C. M. Ko and E. N. Parker, *Astrophys. J.* **341**, 828 (1989).